water

MDPI

Article

Toward a General Analytical Formulation for the Hydrodynamic Behavior of Tesla Valves

Mauricio De la Cruz-Ávila, Mario Ivan Estrada-Delgado, Francisco Javier Castillo Guerrero and Rosanna Bonasia *

School of Engineering and Sciences, Tecnologico de Monterrey, Carretera Lago de Guadalupe Km 3.5 Atizapán de Zaragoza Col. Margarita Maza de Juárez, Cd López Mateos 52926, Mexico; mauricio_dlca@tec.mx (M.D.l.C.-Á.); iestrada@tec.mx (M.I.E.-D.); francisco.cas@tec.mx (F.J.C.G.)

* Correspondence: rosanna.bonasia@tec.mx

Abstract

Tesla valves are passive hydraulic devices capable of producing directional flow resistance without moving components, making them attractive for applications in microfluidics, thermal systems, and high-reliability hydraulic circuits. Despite extensive experimental and numerical studies, an analytical formulation capable of describing the hydrodynamic behavior of Tesla valves under varying operating and geometric conditions remains limited. In this work, a comprehensive analytical model is developed to describe the pressure losses, flow redistribution, and diodicity behavior of Tesla valves through a physics-based formulation derived from conservation laws, dimensional analysis, and inertial scaling principles. The proposed model incorporates the influence of Reynolds number, flow partition, geometric ratios, branch inclination angle, and number of diode stages within a unified nonlinear framework. A closed structural equation is obtained that relates hydraulic losses and directional asymmetry to the internal geometry of the valve. The formulation reveals the existence of geometric and energetic constraints governing rectification efficiency, including bounds associated with stage number, channel scaling, and angular momentum exchange. The results show that Tesla valve performance emerges from a delicate balance between inertial amplification and dissipative mechanisms, providing an analytical framework for the design and optimization of Tesla-type hydraulic systems across multiple scales.

Keywords: Tesla valve; analytical formulation; diodicity; hydraulic losses; flow rectification; passive flow control

Check for updates

Academic Editor: Wencheng Guo

Received: 5 June 2026
Revised: 1 July 2026
Accepted: 2 July 2026
Published: 7 July 2026

Copyright: © 2026 by the authors. Licensee MDPI, Basel, Switzerland. This article is an open access article distributed under the terms and conditions of the Creative Commons Attribution (CC BY) license.

1. Introduction

Tesla valves are based on the work of Nikola Tesla from 1920 [1], who proposed this type of hydraulic device with no moving parts, capable of providing flow resistance based on its direction. This system, now known as a Tesla valve, originated as a passive structure composed of a series of geometric bifurcations that induce flow within a duct. Its most important characteristic is its directional behavior, whereby the fluid encounters much less resistance when moving in the designated forward direction, in contrast to the much more significant energy losses that occur when the flow direction is reversed. This is now known as the diodicity effect, as it is analogous to the behavior of electrical diodes, since the system predicts flow in a preferred direction. The advent and subsequent advancement of experimental hydraulics contributed to the introduction of the diodicity number (D_i) as a dimensionless parameter that quantifies the conventional behavior of this type of

structure [2]. The D_i number [3] is normally determined as the ratio between the pressure drop in the reverse flow direction and the pressure drop under equivalent conditions in the forward flow direction, thus allowing the evaluation of the device's efficiency in discriminating between the two flow directions. This concept subsequently became one of the fundamental parameters for characterizing Tesla valves in experimental, numerical, and analytical studies.

Over the past few decades, interest in these geometric configurations has reemerged due to their potential application in systems where flow control must be achieved without moving mechanical components [4,5], particularly in microfluidics, thermal systems, and high-reliability hydraulic circuits. One of the experimental studies in this context [6], which systematically evaluated the hydrodynamic behavior of a Tesla valve under different Reynolds numbers [7], involved detailed measurements of pressure drop and internal flow structure, allowing the identification of the physical mechanisms responsible for hydraulic asymmetry [8]. The results propose that, when the flow is reversed, extensive boundary layer separation regions and intense vortex structures are generated in the lateral cavities of the device. These structures cause a significant increase in energy dissipation and, consequently, greater hydraulic resistance. In contrast, when the flow is forward, the main flow passes through the conduit with less interaction with the lateral branches, reducing recirculation and decreasing pressure loss. Furthermore, the study showed that the diodicity value increases progressively with the Reynolds number [7], indicating that inertial effects play a dominant role in amplifying hydraulic asymmetry. This result is particularly relevant because it experimentally confirms that the Tesla valve can indeed behave as a passive hydraulic diode, validating hypotheses previously formulated through numerical simulations. However, this work focused primarily on the phenomenological characterization of the flow and the identification of the physical mechanisms associated with energy dissipation, without developing general mathematical models capable of predicting the hydraulic behavior of the system under different geometric configurations.

In parallel, several studies have addressed the analysis of Tesla valves using computational fluid dynamics (CFD) tools [9–12], with the aim of understanding in greater detail the influence of geometry on the hydraulic performance of the device [13]. These investigations have demonstrated that geometric parameters such as the bypass angle of the side channels [14], the aspect ratio of the main conduit, and the number of stages or Tesla modules have a direct influence on the pressure distribution and the diodicity number [2]. Three-dimensional simulations have shown that, as the number of stages in the valve increases, the pressure difference between forward and reverse flow increases significantly. This behavior is due to the successive generation of vortical structures and recirculation zones within each geometric module, which act as additional energy dissipation mechanisms in the reverse flow. In physical terms, each additional stage introduces a new flow diversion and recombination process that intensifies turbulent mixing and increases the loss of kinetic energy. These characteristics have motivated the exploration of Tesla valves in multiple technological applications, particularly in the field of microfluidics, where the absence of moving parts is especially advantageous for small-scale devices [15,16]. Potential applications have also been investigated in heat exchangers [17], passive cooling systems [13,18], and supercritical CO_2 circuits [19], where the ability to control the preferred flow direction can improve the stability and efficiency of thermal systems [20,21].

The literature on Tesla valves has evolved through three broad methodological stages: early studies focused on experimental characterization of diodicity and flow separation [6], followed by CFD-based investigations of geometry-dependent losses and internal flow structures [9–12], and more recently by geometry-specific scaling correlations [15].

However, these contributions remain largely configuration-dependent and have not yet yielded a general analytical formulation.

Despite advances in experimental characterization and understanding of the hydrodynamic mechanisms involved, one of the main challenges in the study of Tesla valves has been the development of predictive mathematical models capable of generally describing the pressure drop in these devices. In this context, one of the most relevant contributions is the work of Liu et al. [15], who proposed a scaling law for the pressure drop in systems composed of multiple symmetrical Tesla valves. Through a combination of CFD simulations and dimensional analysis, the authors identified a functional relationship between the pressure drop, the Reynolds number, the characteristic flow velocity, the number of valves in the system, and the geometric parameters of the conduit. As a result, a logarithmic correlation was obtained that describes the variation in the pressure drop according to the following expression [3],

$$\Delta p \sim \left(1 + \ln\left(1 + N^{3/5} Re^{1/3}\right)\right) \rho V^2 L D^{-1} Re^{-1/4} \quad (1)$$

where N represents the number of Tesla valves or stages, Re is the Reynolds number, ρ is the fluid density, V is the characteristic flow velocity, L is the characteristic length of the system, and D corresponds to the hydraulic diameter of the channel. This formulation constitutes one of the first attempts to establish a scaling law for this type of device, simultaneously integrating geometric and dynamic parameters within a single analytical expression. The development of this correlation represents a significant advance, as it allows for estimating the hydraulic behavior of the system without necessarily resorting to detailed numerical simulations for each particular configuration.

Available studies [22] suggest that the flow dynamics inside a Tesla valve are largely dominated by the following three basic hydrodynamic mechanisms: flow separation, the generation of vortex structures, and turbulent mixing promoted by the channel geometry. It has been observed that the Reynolds number influences the magnitude of the vortex structures generated within the channel [23,24]. As Re increases, inertial forces become more significant, tending to magnify separation and recirculation phenomena. Similarly, the number of stages, the length of the branches, and the connection angles determine the intensity of the recirculating structures and, consequently, the final diodicity value achieved by the system.

Despite the significant progress made in this field over the last decade, the relevant scientific literature also reveals numerous research gaps that still limit a comprehensive understanding of these devices. Firstly, a significant amount of existing work is based on idealized numerical simulations [5,8,25–27], while experimental validation is scarce [6,28], for example, in complex geometric arrangements or highly turbulent flow regimes. Secondly, most proposed models are empirical correlations obtained for a specific geometry, preventing their generalizability to other arrangements. Furthermore, the effects of various physical parameters that are critical in these devices, such as surface roughness, deflection radii, and micro-nano scaling processes, have not been systematically characterized. These parameters affect the flow structure and modify energy losses in the system, particularly in microfluidics applications where characteristic flow lengths are comparable to boundary layer thickness. As a result, there is still no universal equation that describes the behavior of Tesla valves for general operating conditions, which limits their systematic integration into the design of hydraulic systems.

A more fundamental limitation emerges when the available literature is examined from a theoretical perspective. Although extensive experimental measurements, CFD investigations, and geometry-specific correlations have significantly improved the understanding of Tesla valve hydrodynamics, these approaches do not provide a general

analytical formulation capable of explicitly relating geometry, flow redistribution, hydraulic losses, and diodicity within a unified mathematical framework. Consequently, the field remains largely descriptive and configuration-dependent, with predictive capabilities often restricted to the specific geometries and operating conditions under which empirical correlations or numerical simulations were originally developed. To date, a closed analytical equation describing the emergence of directional hydraulic resistance in Tesla valves from first-order hydrodynamic principles remains unavailable.

In response to these limitations, there have been current research trends toward formulating functional relations between fundamental parameters such as the Reynolds number, channel geometric characteristics [29,30], pressure drop, diodicity number, etc., in order to formulate robust scaling laws for predicting the hydraulic behavior of Tesla valves under different operating conditions, thus evolving from a predominantly experimental and phenomenological approach to a theoretical–analytical framework based on the principles of dynamic similarity and scaling analysis.

In this context, the objective of the present work is to develop a generalized analytical framework capable of describing the emergence of diodicity from the coupled interaction between geometry, flow redistribution, and hydraulic dissipation. The proposed formulation seeks to establish a theoretical foundation for Tesla valve hydrodynamics by deriving explicit mathematical relations linking pressure losses, flow partition, geometric parameters, and directional behavior. Consequently, the contribution of this work is primarily analytical in nature, providing a predictive framework whose consistency is evaluated through mathematical rigor, dimensional coherence, and physical interpretability, while experimental and high-fidelity numerical validation remain subjects for future investigation.

Accordingly, the present work should be read as a reduced-order analytical model; quantitative design use will require experimental validation and calibration of the loss coefficients K_c, K_{r0}, K_e and α against high-fidelity CFD or laboratory measurements.

Beyond its analytical formulation, a key contribution of the proposed framework lies in its ability to provide a structured mathematical description of the relationship between geometry and hydrodynamic response. In contrast to existing empirical or semi-empirical approaches, which are often limited to specific configurations and offer limited physical interpretability, the present model explicitly links the governing parameters of the valve to its hydraulic performance.

This explicit formulation enables direct control over the variables that define device behavior, allowing a systematic exploration of how geometric modifications influence flow resistance, energy dissipation, and directional asymmetry. As a result, the model provides a framework for parameter tuning, sensitivity analysis, and design-oriented investigations, all of which are essential for engineering applications.

From a practical perspective, this capability provides a parametric analytical basis for identifying the geometric and hydraulic conditions under which rectification is enhanced or suppressed, enabling systematic parameter-space exploration prior to detailed numerical simulation or experimental implementation. This is particularly relevant in applications beyond microfluidics, where larger-scale hydraulic systems demand precise control over flow regulation and energy losses. In this context, the proposed formulation opens new possibilities for the design of Tesla-type devices in surface hydraulics and other macroscopic flow systems, where customized directional resistance and passive flow control are required.

In this way, the developed model contributes to a generalized analytical description of hydraulic rectification in Tesla valves and provides a theoretical basis for future analysis, numerical investigation, experimental assessment, and engineering design of hydraulic systems based on this type of device.

2. Conceptual Framework of the Model

Describing the hydrodynamic behavior of a Tesla valve needs a conceptual framework that links the dynamic flow variables with the geometric parameters characterizing the mechanism's configuration. Unlike conventional valves, which use moving valve elements to control flow, the Tesla valve relies on an internal geometry where fluid circulation follows different paths depending on the flow path. Therefore, the Tesla valve exhibits a directional hydraulic response, where pressure, energy losses, and the internal flow structure depend on the flow's evolution, which, in turn, depends on the system's geometry. Consequently, formulating the problem requires establishing the parameters that govern the interaction between the flow and the valve's geometry.

From a dynamic perspective, flow behavior is characterized by macroscopic variables related to momentum transport within the channel. These include characteristic flow velocity, fluid density, and viscosity, which determine the flow regime and hydraulic losses. The consideration of these characteristics is typically expressed through the Reynolds number, which represents the ratio between inertial and viscous forces. This dimensionless parameter is fundamental for describing the transitions between different flow regimes and for interpreting the formation of hydrodynamic structures such as flow separation, recirculation, or vortex formation. Simultaneously, the system's final response can be evaluated by the pressure drop that appears along the configuration, a magnitude that describes the energy loss associated with fluid transport within the device.

The system's geometry, as well as the dynamic flow variables, determines the device's hydrodynamic response. Thus, the angle of the baffles; the width of the main channel; the diameter of the secondary channels that integrate the hydraulic diodes; the total number of stages or diodes present in the arrangement; the total length of the valve, etc., define the path that the fluid follows through the system. These geometric characteristics determine the intensity of internal recirculation, the intensity of flow separation behavior, and the redistribution of the velocity field through the channel, resulting in energy losses or hydraulic losses and governing the magnitude of hydraulic rectification.

From this perspective, the fundamental problem lies in obtaining a functional relationship to describe the overall hydrodynamic behavior of the Tesla valve as a function of the interaction between the dynamic flow parameters and the geometric variables that determine the device's configuration. Formulating this relationship is the starting point for constructing an analytical model that can generally incorporate the physical mechanisms governing momentum transport, energy dissipation, and the system's directional response. Thus, the proposed conceptual framework serves as the foundation for developing a general expression that justifies and interprets the hydraulic behavior of Tesla valves under various operating conditions.

2.1. Schematic Diagram of the Tesla Valve

Figure 1 shows a schematic representation of the Tesla valve configuration considered in the present study. The diagram illustrates the principal geometrical elements of the device, including the main flow channel, the sequence of hydraulic diode stages arranged along the streamwise direction, and the lateral derivations that connect the diversion paths with the primary conduit. The inclination angle of the secondary branches relative to the main channel is indicated, together with the characteristic dimensions defining the geometry, such as the width of the primary channel, the hydraulic diameter of the lateral conduits, and the total streamwise length of the configuration.

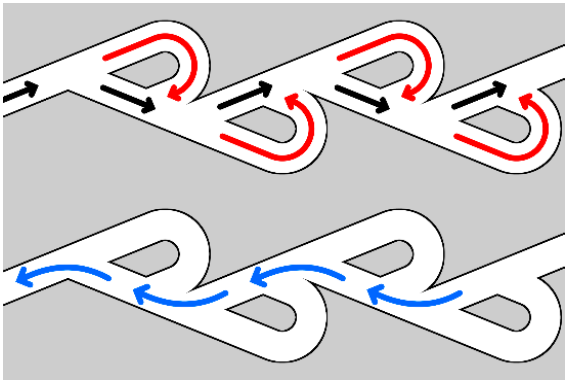


Figure 1. Tesla valve schematic [1]. Red arrows represent the reverse flow direction (high-resistance mode), while blue arrows represent the forward flow direction (low-resistance mode).

In addition, the schematic identifies the number of diode stages that compose the valve and highlights the periodic arrangement of the branching structures that produce directional flow resistance. These geometric parameters constitute the fundamental descriptors of the system and will be used in the subsequent analytical formulation to relate the valve geometry with the resulting pressure drop, Reynolds number dependence, and diodicity of the flow.

2.2. Physical Assumptions of the Model

The analytical formulation proposed in this study is based on a set of physical assumptions that allow the complex hydrodynamic behavior of the Tesla valve to be represented within a tractable mathematical framework. The working fluid is assumed to be incompressible, which is a reasonable approximation for liquid flows and for gas flows under the moderate pressure variations typically encountered in internal hydraulic devices. Under these conditions, density variations are negligible and the continuity equation simplifies to a divergence-free velocity field. In addition, the thermophysical properties of the fluid, particularly density and dynamic viscosity, are assumed to remain constant throughout the domain. This assumption eliminates potential coupling between thermal and momentum transport and allows the flow dynamics to be described solely in terms of the governing momentum balance.

Within this framework, the flow regime inside the valve is interpreted as the result of the interaction between inertial and viscous forces. This balance is commonly characterized by the Reynolds number, which governs the relative importance of convective momentum transport and viscous dissipation. The model, therefore, focuses on capturing how this competition between inertia and viscosity interacts with the asymmetric geometry of the device to generate directional resistance. By emphasizing these dominant physical mechanisms, the formulation seeks to represent the macroscopic hydraulic behavior of the system without resolving the full spatial complexity of the flow field.

A further assumption concerns the hydrodynamic state of the flow in the primary channel. Away from the regions where lateral branches intersect the main conduit, the flow is considered to approach a fully developed condition. This approximation is justified when the streamwise length of the channel segments between successive geometric perturbations is sufficiently large relative to the characteristic hydraulic diameter. Under such circumstances, the velocity profile becomes stable and the local pressure gradient primarily reflects frictional effects along the walls. This simplification provides a consistent baseline description of the core flow, against which the additional perturbations introduced by the valve geometry can be evaluated.

The model assumes hydraulically smooth walls throughout. Wall roughness, deflection radii, and micro–nano boundary-layer effects are not explicitly included in the present formulation; their aggregate influence is implicitly subsumed within the effective loss coefficients K_c, K_{r0}, and K_e, rather than resolved as a function of surface finish or fabrication-dependent geometry. This assumption is particularly noted for microfluidic applications, where characteristic flow lengths may be comparable to boundary layer thickness.

The lateral derivations and reconnection zones introduce abrupt changes in flow direction, local acceleration and deceleration of the fluid, and interaction between the diverted and main streams. As a consequence, a significant portion of the additional hydraulic losses is generated in these geometrically induced disturbances, which act as sources of momentum redistribution and energy dissipation. The present model, therefore, focuses on describing the global hydraulic response of the device by relating these geometrically induced losses to the overall pressure drop and directional resistance of the valve, rather than attempting to resolve every local flow structure within the device.

Three-dimensional flow structures are not explicitly resolved and are represented through effective loss coefficients capturing aggregate dissipative behavior.

For completeness, the principal modeling assumptions of the present formulation are summarized as follows: (i) a fully developed velocity profile at the inlet of each stage; (ii) outlet pressure taken as a reference condition at each stage exit; (iii) hydraulically smooth walls, with roughness effects absorbed into the effective loss coefficients; and (iv) weak hydrodynamic coupling between consecutive stages, with inter-stage interactions represented through cumulative lumped losses rather than explicit boundary-condition transfer between modules.

3. Analytical Formulation of the Tesla Valve Model

In the present study, the analytic formulation developed was formulated with the use of the fundamental conservation laws governing the fluids' motion and their interaction with the geometry of the Tesla valve. The development begins from the conservation laws of mass, momentum, and energy considerations applied to a control volume surrounding one of the diode stages of the valve, which together provide the mathematical framework required to relate the geometric parameters to its hydraulic response. Under conditions of steady flow, the continuity equation defines the redistribution of volumetric flow rates between the main channel of the valve and its lateral derivation(s). Therefore, the total flow entering an appropriate control volume surrounding the junction of the main channel and lateral derivation(s) will consist of flow continuing in the main channel, as well as flow diverted into one or more lateral derivations. The partitioning of the total flow into continuing (primary) and diverted (secondary) streams is described by means of a flow fraction parameter, which indicates the relative proportion of fluid entering the junction via each of these two pathways, thus providing a key intermediate variable used to relate geometrical features of the Tesla valve to fluid dynamic behavior.

3.1. Conservation of Mass at the Bifurcation

The first step of the formulation is based on the conservation of mass applied to the control volume containing the bifurcation between the main channel and the lateral derivation. For an incompressible fluid under steady conditions, the continuity equation reduces to,

$$\frac{\partial \rho}{\partial t} + \nabla \cdot (\rho \mathbf{V}) = 0, \tag{2}$$

Under steady operating conditions, the density does not vary with time, which eliminates the transient term and reduces the equation to $\nabla \cdot (\rho V) = 0$. Integrating this

expression over a control volume and applying the divergence theorem leads to the integral form of the continuity equation,

$$\oint \rho \boldsymbol{V} \cdot \boldsymbol{n} dA = 0. \tag{3}$$

For the bifurcation geometry considered here, the incoming flow splits into two streams: one continuing along the main conduit and another diverted into the lateral branch. Expressing the mass balance in terms of volumetric flow rates gives $\rho Q = \rho Q_m + \rho Q_r$. Since the density ρ is constant, it cancels from the equation, yielding the volumetric conservation relation,

$$Q = Q_m + Q_r, \tag{4}$$

where Q is the incoming volumetric flow rate, Q_m is the flow remaining in the main channel, and Q_r is the portion diverted toward the lateral branch. At the level of the present reduced-order formulation, the internal flow field is represented through the net volumetric exchange between the main conduit and the lateral branch.

To characterize this redistribution, a flow-partition parameter is introduced:

$$\eta = Q_r / Q, \tag{5}$$

where η denotes the effective flow-partition parameter capturing redistribution effects and represents the fraction of flow entering the branch. The introduction of η provides a reduced-order representation of the flow redistribution process, allowing the effects of geometry and hydraulic losses to be incorporated into a single physically interpretable variable. Using this definition, the flow remaining in the main conduit becomes,

$$Q_m = Q(1 - \eta). \tag{6}$$

This parameter plays a central role in the subsequent formulation because it provides a mathematical link between flow redistribution, hydraulic losses, and the geometric configuration of the valve.

3.2. Velocity Relations and Geometric Scaling

The next step consists of expressing the characteristic velocities in the main channel and the lateral branch as functions of the volumetric flow rates and the corresponding cross-sectional areas. The mean axial velocity in the primary channel is defined as,

$$V_0 = Q/A_0 \leftrightarrow (V_0 = Q/(Sh) if rectangular), \tag{7}$$

while the velocity in the lateral branch is $V_r = Q_r / A_r$. Substituting the definition of the partition relation $Q_r = \eta Q$ parameter leads to $V_r = \eta Q / A_r$. In order to relate the velocities to the geometric configuration of the valve, the ratio between the cross-sectional areas of the main channel and the branch is introduced, $\lambda = A_0 / A_r$. λ represents the geometric area ratio between main and lateral channels. Using this definition and the velocity relation for the main channel $V_0 = Q / A_0$, the branch velocity becomes:

$$V_r = \eta \lambda V_0. \tag{8}$$

Equation (8) establishes the first explicit connection between flow partition and geometric scaling, a relationship that becomes central in the subsequent analytical development. This expression shows that the characteristic velocity in the branch increases proportionally with both the diverted flow fraction and the geometric ratio between the two conduits. Consequently, narrower branches or larger diverted fractions increase the local momen-

tum associated with the diverted flow, which is expected to influence the momentum redistribution process at the bifurcation.

3.3. Reynolds Number and Inertial Regime

The present formulation focuses on the inertia-dominated regime that is most relevant for directional hydraulic rectification. The hydrodynamic regime inside the valve is characterized using the Reynolds number, defined in terms of the mean velocity in the primary channel as $Re = \frac{\rho V_0 D_h}{\mu}$.

Substituting the velocity definition $V_0 = Q/A_0$ leads to:

$$Re = \frac{\rho Q D_h}{\mu A_0}, \tag{9}$$

which indicates that Re is directly proportional to the volumetric flow rate for a given geometry. In the present formulation, attention is restricted to inertia-influenced operating conditions, for which the Reynolds number is sufficiently large that inertial contributions become comparable to or larger than viscous contributions in the momentum balance.

In the operating conditions typically encountered in Tesla valves, the Reynolds number is sufficiently large for inertial effects to dominate the momentum balance. Under this assumption, starting from the incompressible Navier–Stokes equations,

$$\rho\left(\frac{\partial \boldsymbol{V}}{\partial t} + (\boldsymbol{V}\cdot\nabla)\boldsymbol{V}\right) = -\nabla p + \mu\nabla^2\boldsymbol{V}, \tag{10}$$

This can be simplified by neglecting the transient term and considering the convective term as the dominant contribution. The characteristic scaling of the inertial term is, therefore,

$$(\boldsymbol{V}\cdot\nabla)\boldsymbol{V} \sim \frac{V^2}{L}, \tag{11}$$

which leads to the proportionality between pressure forces and the square of the velocity magnitude. This inertial scaling is fundamental to the analytical model because it provides the physical basis for the quadratic dependence of pressure losses on characteristic velocity under inertia-dominated operating conditions.

3.4. Energy Balance and Pressure Losses

The pressure variation across a diode stage is evaluated using the mechanical energy equation. For incompressible steady flow between two sections, the Bernoulli relation can be written as:

$$p + \frac{1}{2}\rho V^2 + \rho g z = const \tag{12}$$

When hydraulic losses are included, the pressure drop across the stage becomes:

$$\Delta p = \frac{1}{2}\rho\left(V_1^2 - V_2^2\right) + \Delta p_{loss} \tag{13}$$

For the purposes of the reduced-order formulation, all hydraulic losses are referenced to the characteristic velocity in the main channel, allowing the distributed effects of flow deviation and dissipation to be represented through equivalent loss coefficients:

$$\Delta p = \Sigma K \frac{\rho V_0^2}{2} \tag{14}$$

This directly reveals the quadratic dependence of pressure losses on the characteristic velocity, leading to the scaling relation $\Delta p \propto V_0^2$. Since V_0 scales linearly with

the volumetric flow rate, the formulation further implies $\Delta p \propto Q^2$. These scaling relations constitute the characteristic pressure-loss behavior expected under inertia-dominated operating conditions.

3.5. Momentum Balance at the Branching Region

To determine the relationship between the diverted flow fraction and the pressure variation across the bifurcation, the integral momentum equation is applied along the streamwise direction,

$$\sum F_x = \oint \rho V_x (\boldsymbol{V} \cdot \boldsymbol{n}) dA. \tag{15}$$

Under the assumptions of the present reduced-order formulation, pressure forces are assumed to provide the dominant contribution to the streamwise momentum balance, while viscous stresses are represented through the equivalent hydraulic losses introduced previously. Consequently, the momentum fluxes associated with the incoming flow, the flow remaining in the main conduit, and the diverted flow entering the branch can be expressed in terms of the corresponding volumetric flow rates and cross-sectional areas. After expressing the velocities in terms of the volumetric flow rates and substituting the relations derived previously, the equation becomes,

$$\rho \frac{Q^2}{A_0} - \rho \frac{Q^2 (1-\eta)^2}{A_0} - \rho \frac{Q^2 \eta^2}{A_r} \cos\theta = \Delta p A_0. \tag{16}$$

θ is the branch inclination angle governing directional asymmetry. Dividing by the characteristic inertial term $\rho Q^2 / A_0$ yields a dimensionless expression:

$$1 - (1-\eta)^2 - \eta^2 \lambda \cos\theta = \Phi, \tag{17}$$

where the dimensionless pressure parameter is defined as:

$$\Phi = \frac{A_0^2}{\rho Q^2} \Delta p \tag{18}$$

This definition allows the pressure variation to be expressed relative to the characteristic inertial scale of the flow. Expanding the quadratic term $(1-\eta)^2$ leads to:

$$(1 + \lambda \cos\theta)\eta^2 - 2\eta + \Phi = 0, \tag{19}$$

which constitutes the governing flow-partition equation of the present analytical formulation for a single Tesla-diode stage. Φ represents the dimensionless pressure parameter associated with the total hydraulic losses across the diode stage.

3.6. Extension to Multiple Stages

A Tesla valve is composed of multiple diode stages arranged sequentially along the main conduit. Under the assumption that each stage operates under equivalent hydraulic conditions and that inter-stage interactions can be represented through an equivalent cumulative loss mechanism, the total pressure drop is approximated as the sum of the contributions of the individual stages. If each stage produces a pressure drop Δp_{et}, the total pressure drop across the system containing N identical stages becomes,

$$\Delta p_N = N \Delta p_{et}. \tag{20}$$

This is a first-order approximation: inter-stage hydrodynamic coupling is neglected under a weak-interaction assumption. The outlet pressure of each stage is taken as the

reference inlet condition for the subsequent module, which constitutes an idealization rather than a verified decoupling of the hydrodynamic boundary conditions between consecutive stages. Furthermore, the assumption of equivalent hydraulic conditions across stages implies that local recirculation structures generated within one module do not modify the inlet boundary conditions of the subsequent stage. This idealization is expected to hold in regimes where inertial redistribution between stages remains weak and constitutes a known limit of the present formulation for large N or high-Re configurations.

Using the loss-coefficient representation of the pressure drop, this relation can be written as:

$$\Delta pN = N\Sigma K_{et}\frac{\rho V^2}{2}. \tag{21}$$

By combining Equation (18) with the pressure-loss formulation of Equation (21), the corresponding dimensionless pressure parameter for a valve composed of N identical stages becomes,

$$\Phi_N = \frac{N\Sigma K_{et}}{2}. \tag{22}$$

Substituting this expression into Equation (19) yields the global relation governing the flow partition in a valve with N stages:

$$(1+\lambda\cos\theta)\eta^2 - 2\eta + \frac{N\Sigma K_{et}}{2} = 0. \tag{23}$$

This equation establishes the analytical relationship between flow partition, hydraulic losses, and the principal geometric parameters of the valve, including the area ratio, branch inclination angle, and number of diode stages.

3.7. Hydraulic Loss Model for a Tesla Diode Stage

Having established the equation that relates the flow-partition parameter η with the dimensionless pressure parameter Φ, the next step of the formulation consists of describing the hydraulic losses generated within a Tesla diode stage. In hydraulic systems, pressure losses produced by local geometric perturbations are commonly represented through dimensionless loss coefficients. The total loss coefficient associated with a single diode stage can, therefore, be written as:

$$\Sigma K_{et} = \sum K_i, \tag{24}$$

where the summation accounts for the different physical mechanisms contributing to energy dissipation within the module.

In the Tesla geometry, these contributions arise from several distinct processes associated with the branching and recombination of the flow. The total loss coefficient can, therefore, be decomposed into individual components corresponding to contraction, expansion, flow interaction, and residual dissipation mechanisms. Within the reduced-order framework adopted here, the dominant dissipation mechanisms are represented through a limited set of equivalent hydraulic-loss contributions. This decomposition can be written as:

$$\Sigma K_{et} = K_c + K_{r0} + K_e + K_{impact} \tag{25}$$

where K_c represents contraction losses, K_e corresponds to expansion losses during reinjection into the main channel, K_{impact} describes the additional dissipation generated by the interaction between the returning branch flow and the main stream, and K_{r0} represents a baseline equivalent-loss coefficient that accounts for residual dissipation mechanisms not explicitly represented by the contraction, expansion, and impact terms. The additive representation adopted here should be interpreted as an equivalent hydraulic-loss

decomposition rather than a strict separation of independent physical processes. Under the inertia-dominated conditions considered in the present formulation, this coefficient is assumed to be approximately independent of Reynolds number and, therefore, represents an averaged contribution of viscous and turbulent dissipation mechanisms.

3.8. Angular Impact Losses in the Branch Interaction

Among these contributions, the impact term plays a particularly important role because it directly depends on the orientation of the lateral branch relative to the main flow direction. When the diverted flow re-enters the primary channel, its velocity component normal to the main flow produces a momentum exchange that generates additional dissipation. This effect can be expressed as proportional to the square of the branch velocity projected onto the direction perpendicular to the main flow. Since the dissipation associated with the impact process scales with the kinetic energy of the velocity component normal to the main flow, the dependence appears as $\sin^2\theta$. The scaling of the impact loss term, therefore, is as follows:

$$K_{impact} \propto \frac{V_r^2}{V_0^2}\sin^2\theta \tag{26}$$

where V_r is the characteristic velocity in the lateral branch and θ is the inclination angle between the branch and the main conduit. Substituting the previously derived velocity relation for the branch,

$$V_r = \eta\lambda V_0, \tag{27}$$

$$\frac{V_r^2}{V_0^2} = (\eta\lambda)^2 \tag{28}$$

The impact term becomes proportional to

$$K_{impact} \propto (\eta\lambda)^2 sin^2\theta, \tag{29}$$

which explicitly reveals the dependence of the impact losses on the diverted flow fraction, the geometric area ratio between conduits, and the inclination angle of the branch. The impact loss coefficient is formulated by normalizing the branch kinetic energy with respect to the dynamic pressure of the main flow, ensuring dimensional consistency.

Introducing a proportionality constant α to represent the efficiency of the momentum exchange process, the impact contribution can be written in closed form as:

$$K_{impact} = \alpha(\eta\lambda)^2 sin^2\theta, \tag{30}$$

The impact loss term is introduced as a scaling-based closure, capturing the momentum exchange generated by the oblique reinjection of the branch flow into the main stream. The coefficient α represents an effective momentum-exchange efficiency factor associated with the branch reinjection process. Although its value may depend on the Reynolds number and geometric characteristics, it is introduced here as a lumped parameter intended to capture the cumulative effect of unresolved interaction mechanisms. It may ultimately be quantified through calibration, detailed numerical simulations, or experimental measurements depending on the specific application. This formulation preserves analytical tractability while incorporating the dominant nonlinear interaction between geometry and flow redistribution.

This expression provides a compact representation of the dominant nonlinear interaction between the geometric parameters of the diode and the flow redistribution occurring

at the bifurcation. Substituting this result into the loss decomposition yields the complete loss-coefficient expression adopted for a single diode stage,

$$\boxed{\Sigma K_{et} = K_c + K_{r0} + K_e + \alpha(\eta\lambda)^2 \sin^2\theta} \tag{31}$$

which constitutes the closure relation adopted in the present analytical formulation linking hydraulic losses with the geometric configuration of the valve. Substituting the loss model into the definition of the dimensionless pressure parameter yields:

$$\Phi = \frac{\left[K_c + K_{r0} + K_e + \alpha(\eta\lambda)^2 sin^2\theta\right]}{2} \tag{32}$$

3.9. Coupled Equation of the System

The final step of the derivation consists of substituting the dimensionless pressure parameter Φ_N into the equation obtained previously for the bifurcation dynamics. This substitution leads to:

$$(1 + \lambda\cos\theta)\eta^2 - 2\eta + \frac{N\Sigma K_{et}}{2} = 0 \tag{33}$$

which expresses the coupling between the flow-partition parameter and the cumulative pressure losses generated by the valve geometry. Replacing the explicit expression for the stage loss coefficient $N\Sigma K_{et}$ produces the fully expanded equation:

$$(1 + \lambda\cos\theta)\eta^2 - 2\eta + \frac{N}{2}\left[K_c + K_{r0} + K_e + \alpha(\eta\lambda)^2 \sin^2\theta\right] = 0. \tag{34}$$

Since the impact-loss contribution is proportional to η^2, the governing equation preserves its quadratic structure in the flow-partition variable. Rearranging the terms to group the quadratic contributions in η^2 yields:

$$\eta^2\left[(1 + \lambda\cos\theta) + \frac{N}{2}\alpha\lambda^2\sin^2\theta\right] - 2\eta + \frac{N}{2}(K_c + K_{r0} + K_e) = 0. \tag{35}$$

The existence of a physically admissible solution requires $0 < \eta < 1$, which imposes additional constraints on the combinations of geometric and hydraulic parameters considered by the model. This equation constitutes the closed form of the analytical model, relating the flow partition within the valve to the combined effects of geometry, stage number, and hydraulic loss mechanisms. Since the impact-loss contribution is proportional to η^2, the governing equation preserves its quadratic structure in the flow-partition variable.

3.10. Forward-Flow Condition

The forward-flow configuration is defined here as the operating condition in which flow diversion into the lateral branches contributes minimally to the overall flow redistribution. Under this condition, the geometry of the diode elements promotes only limited diversion of the flow toward the lateral branches. As a consequence, the fraction of flow entering the derivations becomes sufficiently small such that $\eta_f \to 0$ is adopted as a first-order approximation.

This limit simplifies the expression of the total loss coefficient associated with a diode stage. Since the diverted velocity becomes negligible, the nonlinear angular interaction term disappears and the loss coefficient reduces to the baseline hydraulic-loss contributions represented by $K_c + K_{r0} + K_e$. The effective loss coefficient in forward flow can, therefore, be approximated as $\Sigma K_{et,f} \approx K_c + K_{r0} + K_e$. Under this condition, the pressure drop generated

by a valve containing N identical stages can be obtained by substituting this coefficient into the general pressure-loss formulation,

$$\Delta p_f = N(K_c + K_{r0} + K_e)\frac{\rho V_0^2}{2}. \tag{36}$$

This expression shows that the pressure drop in the forward direction is governed primarily by the baseline hydraulic-loss mechanisms associated with contractions, expansions, and weak recirculation regions. No additional losses associated with angular momentum exchange appear because the diverted flow component is essentially suppressed. This forward-flow limit, therefore, establishes the reference hydraulic state against which the reverse-flow condition and the resulting diodicity are subsequently evaluated.

3.11. Reverse-Flow Condition

Tesla valves develop their characteristic hydraulic resistance. In this regime, the geometric arrangement of the diode elements promotes a significant redistribution of the flow into the lateral branches. The diverted fluid subsequently returns toward the main conduit, where it interacts with the primary flow and modifies the local flow topology. This interaction modifies the local flow topology, promoting enhanced recirculation, flow separation, and momentum redistribution processes that are characteristic of reverse operation.

Under these conditions, the total loss coefficient associated with a diode stage includes both the hydraulic losses generated by the modified reverse-flow topology and the additional dissipation associated with the oblique reinjection of the diverted flow. The loss coefficient can, therefore, be written as:

$$\Sigma K_{et,r} = K_c' + K_{r0,r} + K_e' + \alpha(\eta_r \lambda)^2 sin^2\theta \tag{37}$$

where the primed coefficients represent effective contraction, recirculation, and expansion losses associated with the reverse-flow topology. These coefficients differ from their forward-flow counterparts because the fluid experiences a different sequence of flow redirection, separation, and recombination processes when traversing the valve in the reverse direction. The final term corresponds to the additional momentum-exchange dissipation generated when the branch flow re-enters the main channel at an oblique angle.

In the present formulation, directional asymmetry emerges from the combined effect of the modified reverse-flow topology represented by the primed loss coefficients and the additional angular interaction term. Together, these mechanisms increase the overall hydraulic resistance of the valve under reverse-flow conditions while preserving the same general analytical framework used for the forward-flow configuration.

Using this loss coefficient, the total pressure drop in reverse flow for a valve containing N stages can be expressed as:

$$\Delta p_r = N\Sigma K_{et,r}\frac{\rho V_0^2}{2} \tag{38}$$

This formulation highlights the fundamental physical mechanisms underlying Tesla valve operation. Under reverse-flow conditions, the modified flow topology promotes enhanced contraction, recirculation, and expansion losses, while the oblique reinjection of the diverted flow introduces an additional momentum-exchange dissipation mechanism. The combined action of these effects increases the hydraulic resistance of the valve and gives rise to directional asymmetry.

3.12. Energetic Asymmetry of the Valve

The operational principle of the Tesla valve emerges directly from the difference between the pressure losses generated under reverse-flow and forward-flow conditions.

Using the expressions previously obtained for both configurations, the energetic asymmetry of the valve can be evaluated by subtracting the forward-flow pressure drop from the reverse-flow pressure drop. Substituting Equations (36) and (38) yields:

$$\Delta p_r - \Delta p_f = N\left[\left(K_c' - K_c\right) + \left(K_{r0,r} - K_{r0}\right) + \left(K_e' - K_e\right) + \alpha(\eta_r\lambda)^2\sin^2\theta\right]\frac{\rho V_0^2}{2}. \quad (39)$$

Equation (39), therefore, shows that the energetic asymmetry is not solely a consequence of geometric directionality, but rather emerges from the combined action of topology-dependent hydraulic losses and flow-redistribution effects. The relative importance of each contribution depends on the operating conditions and geometric characteristics of the valve.

For the particular case in which the directional variations in the baseline hydraulic-loss coefficients are assumed to be small compared with the angular interaction mechanism, Equation (39) reduces to:

$$\Delta p_r - \Delta p_f = N\alpha(\eta_r\lambda)^2\sin^2\theta\frac{\rho V_0^2}{2} \quad (40)$$

This simplified expression isolates the contribution of the momentum-exchange mechanism and explicitly reveals the influence of the number of stages, the diverted-flow fraction, and the branch inclination angle on the directional hydraulic response of the valve. Since the characteristic velocity in the primary channel is given by $V_0 = Q/A_0$, both Equations (39) and (40) predict that the energetic asymmetry scales with the square of the volumetric flow rate. Consequently, $\Delta p_r - \Delta p_f \propto NQ^2$, indicating that directional resistance increases quadratically with flow rate. This scaling reflects the inertia-dominated nature of the dissipation mechanisms responsible for hydraulic rectification within the Tesla valve.

3.13. Hydraulic Diodicity

A convenient dimensionless measure of the directional behavior of the valve is the diodicity coefficient, defined as the ratio between the hydraulic losses in reverse and forward flow, $D = \Sigma K_r/\Sigma K_f$ Substituting the expressions obtained for the loss coefficients yields the complete analytical expression,

$$D = \frac{K_c' + K_{r0,r} + K_e' + \alpha(\eta_r\lambda)^2 sin^2\theta}{K_c + K_{r0} + K_e}. \quad (41)$$

This relation shows that directional amplification emerges from the combined effect of the modified reverse-flow hydraulic-loss coefficients and the additional momentum-exchange dissipation associated with oblique flow reinjection. The resulting diodicity depends on the geometric characteristics of the valve, the flow-partition parameter, and the effectiveness of the momentum-exchange mechanism represented by α.

An important consequence of the formulation is that the influence of the number of stages is not introduced directly into the diodicity expression but indirectly through its effect on the flow-partition parameter obtained from the coupled governing equation. Consequently, if the flow-partition parameter remains approximately unchanged as stages are added, both forward and reverse pressure losses scale similarly with N and the resulting diodicity remains approximately constant. However, because η is itself governed by the nonlinear system equation, variations in stage number may modify the flow redistribution process and, therefore, influence the directional amplification predicted by the model.

This result suggests that increasing the number of stages primarily amplifies the overall hydraulic resistance of the valve, while changes in directional performance depend on how the additional stages modify the underlying flow-partition mechanism.

3.14. Geometric Scaling Effects

The analytical formulation also provides insight into how geometric scaling influences flow redistribution within the valve. For a rectangular channel, the cross-sectional area of the main conduit can be expressed as $A_0 = S{\cdot}h$, where S represents the characteristic channel width and h the channel depth. The analytical formulation also provides insight into how geometric scaling influences flow redistribution within the valve. For a rectangular channel, the cross-sectional area of the main conduit can be expressed as h, the channel depth. Under this representation, the area ratio between the main conduit and the lateral branch is defined as $\lambda = A_0/A_r$, indicating that modifications of the main-channel dimensions directly influence the geometric parameter governing flow partition.

At the same time, the mean velocity in the primary conduit is given by $V_0 = Q/A_0$. Therefore, for a fixed flow rate, increasing the cross-sectional area of the main conduit reduces the characteristic flow velocity. This relationship demonstrates that geometric scaling affects both the hydraulic transport capacity of the primary channel and the relative importance of the branch-flow contribution within the overall redistribution process.

Inspection of the governing equation further indicates that the effectiveness of flow diversion depends on the balance between the geometric ratio λ, the flow-partition parameter η, and the nonlinear interaction mechanisms represented by the loss model. As the main conduit becomes progressively larger relative to the lateral branch, the contribution of the diverted flow to the overall momentum redistribution process tends to become less significant. Consequently, the angular interaction term associated with branch reinjection exerts a weaker influence on the global hydraulic response predicted by the model.

Within the present analytical framework, this behavior suggests that excessively large area ratios reduce the effectiveness of the flow-redistribution mechanism responsible for directional asymmetry. As a result, the hydraulic response approaches that of a conventional conduit in which most of the flow remains confined to the primary channel and only a limited fraction participates in the branch-induced dissipation processes.

This scaling analysis highlights the importance of maintaining an appropriate geometric balance between the main channel and the lateral branches in order to preserve the flow-redistribution mechanisms that generate directional hydraulic behavior. The results, therefore, suggest that geometric scaling influences valve performance not only through changes in hydraulic resistance but also through its effect on the underlying redistribution–dissipation equilibrium governing diodicity.

3.15. Expanded Structural Equation Including Geometric Losses

The coefficient ΣK_{et} represents the total dimensionless hydraulic loss associated with a single Tesla diode stage and is obtained as the sum of the individual dissipative mechanisms acting within that stage. Replacing the expression for the stage loss coefficient derived previously leads to the fully expanded quadratic equation governing the system in Equation (35). This expression explicitly shows how the redistribution of flow depends on the combined effects of geometry and hydraulic losses. The first term represents the inertial coupling between the main stream and the diverted flow. The second term arises directly from the continuity constraint, while the final term incorporates the cumulative hydraulic losses generated by contraction, recirculation and expansion processes inside

each diode stage. For clarity of analysis, the previous Equation (35) can be written in the standard quadratic form:

$$a\eta^2 + b\eta + c = 0 \tag{42}$$

where the coefficients of the polynomial are defined as:

$$\begin{gathered} a = (1 + \lambda\cos\theta) + \tfrac{N}{2}\alpha\lambda^2\sin^2\theta \\ b = -2 \\ c = \tfrac{N}{2}(K_c + K_{r0} + K_e) \end{gathered} \tag{43}$$

These coefficients reveal the consistent structure of the model. The parameter a combines the geometric effect of the bifurcation orientation with the nonlinear contribution produced by the branch interaction term. The parameter b arises directly from the mass-conservation constraint, while c represents the accumulated hydraulic losses generated by the internal structures of the valve. Among the two mathematical roots of Equation (42), the physically admissible solution is selected as the branch that simultaneously satisfies the asymptotic condition $\eta \to 0$ as the hydraulic losses vanish $(c \to 0)$ and the admissibility constraint $0 < \eta < 1$. This branch is, therefore, consistent with the limiting forward-flow regime and is adopted throughout the subsequent analysis.

The validity of the model requires that the quadratic equation governing the flow partition admits real solutions. This requirement follows from the fact that the parameter η represents a measurable flow fraction and must, therefore, remain within the real domain. For a quadratic equation of the form of Equation (42), real solutions exist only when the discriminant satisfies $\Delta = b2 - 4ac \geq 0$. Substituting the coefficients obtained previously yields

$$\Delta = 4 - 4\left[(1 + \lambda\cos\theta) + \frac{N}{2}\alpha\lambda^2\sin^2\theta\right]\frac{N}{2}(K_c + K_{r0} + K_e) \tag{44}$$

The condition $\Delta \geq 0$ defines the admissible region of parameter space in which the analytical formulation yields physically interpretable solutions for the flow-partition parameter.

An important consequence of this condition is the emergence of an upper bound on the number of diode stages that can be represented within the assumptions of the present formulation. For a fixed set of geometric and hydraulic parameters, increasing N modifies the coefficients of the governing equation and may eventually lead to $\Delta < 0$. Under such conditions, the flow-partition variable no longer admits real-valued solutions within the analytical framework.

This result should not be interpreted as a physical impossibility of Tesla valve operation. Rather, it indicates that the flow-partition representation adopted in the present model is no longer self-consistent for that combination of parameters. The discriminant condition, therefore, establishes a mathematical limit of applicability of the formulation and defines the admissible domain within which physically interpretable solutions exist.

The emergence of this admissibility condition is a direct consequence of the nonlinear coupling between geometry, hydraulic losses, and flow redistribution. Consequently, the formulation predicts that these quantities cannot vary independently but remain constrained by the mathematical structure of the governing equation.

3.16. Analytical Limits and Asymptotic Behavior of the Model

3.16.1. Structural Solution

The analytical development presented earlier results in a quadratic formulation for the flow-partition parameter η, arising from the integral momentum balance at the bifurcation region of the Tesla diode element. The fundamental structure of this relationship is given in

Equation (19). By further incorporating the stage loss coefficient derived in the preceding section, the model is extended to its complete form, as expressed in Equation (35), which includes the contribution of distributed losses and geometrical parameters associated with the multi-stage configuration.

As discussed previously for the forward-flow limit, the diverted flow fraction becomes sufficiently small such that $\eta_f \to 0$ can be adopted as a first-order approximation. Under this limit, the flow diversion becomes sufficiently small, and the hydraulic losses associated with the diode element reduce to the purely geometric contributions, $\Sigma K_{et,f}$. This regime corresponds to the low-resistance state of the Tesla valve, where the flow propagates primarily through the main conduit with minimal interaction with the branch structures. In the reverse-flow configuration, the physically admissible branch of the analytical solution is given by,

$$\eta_r = \frac{2 - \sqrt{4 - 4ac}}{2a} \tag{45}$$

This is provided that the discriminant remains non-negative. Under this condition, the governing equation admits real-valued solutions for the flow-partition parameter. The resulting value of η depends on the specific combination of geometric and hydraulic parameters and determines the extent of flow redistribution into the lateral branches. As η increases, the angular interaction term remains active and contributes to the additional dissipation mechanisms associated with directional asymmetry. Consequently, the directional response of the valve emerges from the coupled interaction between flow redistribution, hydraulic losses, and geometric forcing represented by the analytical formulation.

The discriminant condition $\Delta \geq 0$, therefore, defines the admissible region of parameter space in which the formulation yields physically interpretable solutions. This admissibility requirement constitutes an intrinsic mathematical constraint of the model and establishes the range of geometric and hydraulic conditions for which the flow-partition representation remains self-consistent.

Additional insight into the structure of the formulation can be obtained by considering asymptotic parameter limits. For sufficiently large values of the geometric ratio λ, the coefficient a becomes dominated by the angular-interaction contribution, $a \approx \frac{N}{2}\alpha\lambda^2\sin^2\theta$. The coefficient a also becomes dominated by the angular-interaction contribution, $\eta \sim \frac{2}{a}$, and, therefore, $\eta \propto \frac{1}{\lambda^2}$. This result indicates that, as the main-channel area becomes increasingly large relative to the branch area, the flow diverted into the lateral branch progressively decreases. Consequently, the effectiveness of the flow-redistribution mechanism weakens and the contribution of the angular interaction term becomes progressively less significant.

A second limiting case is obtained by considering the formal limit $N \to 0$. Although this condition does not correspond to a physical Tesla valve, it provides useful insight into the mathematical structure of the governing equation. In this limit, the cumulative hydraulic-loss contribution vanishes and Equation (34) reduces to:

$$\eta^2(1 + \lambda\cos\theta) - 2\eta = 0, \tag{46}$$

which admits the solutions $\eta = 0$ and

$$\eta = \frac{2}{1 + \lambda\cos\theta}. \tag{47}$$

This limiting behavior shows that, in the absence of accumulated stage losses, the flow-partition process is governed exclusively by the bifurcation geometry. The result highlights the distinct roles played by geometry and hydraulic dissipation within the formulation and provides a useful reference state for interpreting the influence of stage accumulation in the complete model.

3.16.2. Large-N Limit and Critical Stage Number

When the number of diode stages becomes large, the coefficients of the governing quadratic equation scale as:

$$\begin{aligned} a &\sim \tfrac{N}{2}\alpha\lambda^2\sin^2\theta, \\ c &\sim \tfrac{N}{2}(K_c + K_{r0} + K_e). \end{aligned} \tag{48}$$

Consequently, for a fixed set of geometric and hydraulic parameters, the product ac increases approximately as N^2. As the number of stages increases, the discriminant of the governing equation may eventually approach zero and subsequently become negative. Under such conditions, the analytical formulation no longer admits real-valued solutions for the flow-partition parameter, indicating that the corresponding parameter combination lies outside the admissible domain of the model. The limiting condition is obtained by imposing the boundary of admissibility, $\Delta = 0$, which, for the present quadratic formulation with $b = -2$, is equivalent to the condition $ac = 1$. The condition ac ≤ 1 arises from the requirement of real-valued solutions in the quadratic formulation and should be interpreted strictly as a mathematical admissibility constraint of the model.

Using the asymptotic large-N expressions for the coefficients yields the estimate:

$$N_{crit} \approx \frac{2}{\alpha\lambda^2\sin^2\theta(K_c + K_{r0} + K_e)} \tag{49}$$

which defines a characteristic critical stage number associated with the analytical framework.

This result should be interpreted as a mathematical property of the formulation rather than as a physical limitation of Tesla valve operation. The predicted value of (N_{crit}) identifies the approximate boundary beyond which the flow-partition representation adopted in the present model ceases to remain self-consistent. Consequently, the formulation predicts that the number of stages, geometric forcing, and hydraulic losses cannot vary independently, but remain constrained by the admissibility condition arising from the nonlinear structure of the governing equation. Physically, (N_{crit}) may be interpreted as a characteristic threshold beyond which additional stages are expected to provide progressively smaller gains in rectification relative to the accompanying increase in hydraulic losses and geometric complexity. Values exceeding (N_{crit}) are not prohibited, nor do they imply that Tesla valves cease to operate. Rather, they indicate conditions under which the assumptions underlying the present flow-partition description become increasingly restrictive and the practical benefits of additional stages may become less significant. Therefore, (N_{crit}) should be interpreted as a design-oriented analytical threshold associated with diminishing returns rather than as a strict physical constraint on valve construction or operation.

3.16.3. Structural Properties of the Analytical Solution

The analytical formulation also provides insight into several limiting and structural properties of the governing equation. The geometric ratio between the main conduit and the lateral branch can be expressed as $\lambda = \frac{S \cdot h}{A_r}$, where S represents the characteristic width of the primary channel. As the channel width increases, the geometric ratio also increases. Consistent with the asymptotic behavior obtained previously, the flow-partition parameter decreases and tends toward zero as λ becomes sufficiently large. Under these conditions, flow diversion into the lateral branches becomes progressively weaker and the angular interaction term loses significance, reducing the directional response predicted by the model.

The formulation also provides insight into the influence of flow rate. The pressure drop generated by the valve scales according to $\Delta p \propto Q^2$, reflecting the inertia-dominated nature of the dissipation mechanisms represented in the model. However, the dimensionless

pressure parameter is defined as $\Phi_N = \frac{N\Sigma K_{et}}{2}$, which does not explicitly depend on the volumetric flow rate under the assumptions of the present formulation. Consequently, in the inertia-dominated regime, the flow-partition parameter is governed primarily by geometric and hydraulic-loss parameters rather than by the magnitude of the imposed flow rate. This result suggests that flow redistribution becomes approximately independent of Q once inertial scaling dominates the hydraulic response.

Additional information can be obtained by examining the structure of the governing polynomial, $f(\eta) = a\eta^2 - 2\eta + c$. Differentiating with respect to η yields $\frac{d}{d\eta}(a\eta^2 - 2\eta + c) = 2a\eta - 2$. The stationary point of the quadratic form is, therefore, located at $\eta = \frac{1}{a}$. Because admissible geometries satisfy $a > 0$, the quadratic function remains convex and possesses a unique minimum. This property contributes to the well-defined mathematical structure of the analytical formulation and supports the existence of a unique physically admissible solution branch within the admissible parameter domain.

4. Energy Scaling Laws of the Tesla Valve

The following results should be interpreted as analytical predictions derived from the proposed closure assumptions and not as experimentally validated performance limits. The previous section established the mathematical structure of the model, including the existence conditions, asymptotic limits, and stability constraints associated with the flow-partition parameter. The purpose of the present section is different. Rather than analyzing the structural properties of the governing equation, the following development focuses on the energetic consequences of the model and the scaling laws governing pressure losses, diodicity, and design constraints in Tesla valves.

4.1. Base Energetic Scaling

Under the operating conditions of interest, hydraulic losses are assumed to be dominated by inertial mechanisms, leading to a quadratic dependence of pressure drop on the volumetric flow rate. The starting point for the energetic interpretation of the model is the classical formulation of pressure losses in internal flows, as expressed in Equation (14). Using the continuity relation, $V_0 = Q/A_0$, the pressure drop can be rewritten as:

$$\Delta p = \Sigma K \frac{\rho}{2}\left(\frac{Q}{A_0}\right)^2. \tag{50}$$

This expression suggests the fundamental scaling law of the system, $\Delta p \propto Q^2$, indicating that the hydraulic response of the Tesla valve is governed by inertial effects in the regime of interest.

Forward and Reverse Energetic Separation

The directional behavior of the valve emerges from the difference in loss coefficients between forward- and reverse-flow configurations. The corresponding pressure drops can be written as:

$$\Delta p_f = \Sigma K_f \frac{\rho}{2}\left(\frac{Q}{A_0}\right)^2, \tag{51}$$

$$\Delta p_r = \Sigma K_r \frac{\rho}{2}\left(\frac{Q}{A_0}\right)^2. \tag{52}$$

Taking the ratio of these expressions leads directly to the diodicity coefficient, $D = \frac{\Sigma K_r}{\Sigma K_f}$, which confirms that, under inertial conditions, the directional behavior of the valve is independent of the volumetric flow rate. When scaling with main channel area, the cross-sectional area of the main channel can be expressed as $A_0 = S{\cdot}h$, and substituting this

relation into the pressure expression yields $\Delta p \propto \frac{Q^2}{S^2 \cdot h^2}$. This result shows that increasing the width of the main channel reduces the pressure drop quadratically. From a design perspective, this introduces a direct trade-off between hydraulic resistance and compactness.

For the geometric scaling through the area ratio, the governing the interaction between the main channel and the lateral branches is defined as $\lambda = \frac{A_0}{A_r}$, which implies $\lambda \propto S$. The angular loss term appearing in the model, $\alpha(\eta\lambda)^2 sin^2\theta$, scales as $\propto \eta^2 S^2$. However, from the solution derived previously, $\eta \propto \frac{1}{\lambda^2}$, which leads to $(\eta\lambda)^2 \propto \frac{1}{\lambda^2}$. This result reveals a non-trivial scaling behavior: although the geometric ratio increases with channel width, the effective angular contribution decreases. Consequently, if the main channel becomes excessively wide, the angular interaction term cancels out and the model predicts a progressive reduction in directional behavior. The cumulative loss coefficients scale linearly with the number of diode stages,

$$\Sigma K_f = N(K_c + K_{r0} + K_e), \tag{53}$$

$$\Sigma K_r = N\Big[(K_c + K_{r0} + K_e) + \alpha(\eta\lambda)^2 \sin^2\theta\Big]. \tag{54}$$

Substituting into the pressure expression yields $\Delta p \propto NQ^2$, indicating that the overall hydraulic resistance increases linearly with the number of stages. However, the diodicity does not scale linearly with N, because the flow-partition parameter η depends on N through the nonlinear structural equation. This introduces a coupling between geometry and cumulative losses that limits the effectiveness of increasing the number of stages. In the asymptotic regime for a small number of stages, in the limit $N \ll 1$, the coefficients reduce to $a \approx 1 + \lambda\cos\theta$, which yields $\eta \approx \frac{2}{a}$. Substituting into the diodicity expression leads to:

$$D \approx 1 + \frac{\alpha\lambda^2 \sin^2\theta}{K_c + K_{r0} + K_e}\left(\frac{2}{a}\right)^2. \tag{55}$$

This regime is dominated by purely geometric effects, where the directional behavior is controlled primarily by the inclination angle and the area ratio.

In the asymptotic regime for large number of stages, when the number of stages increases, the coefficients scale as $a \propto N$, $c \propto N$, which implies $ac \propto N^2$. The existence condition for real solutions, $ac \leq 1$, introduces a critical number of stages,

$$N_{crit} \sim \frac{2}{\alpha\lambda^2 \sin^2\theta(K_c + K_{r0} + K_e)}. \tag{56}$$

Beyond this limit, the discriminant becomes negative and the model ceases to represent a model-consistent flow configuration. This result proposes that increasing the number of stages indefinitely does not improve performance and may instead lead to loss of physical coherence.

4.2. Combined Scaling with Q, S, and N

The global expression for the reverse pressure drop can be written as:

$$\Delta p_r = N\Big[(K_c + K_{r0} + K_e) + \alpha(\eta\lambda)^2 \sin^2\theta\Big]\frac{\rho}{2}\left(\frac{Q}{S \cdot h}\right)^2. \tag{57}$$

This expression makes explicit the combined scaling behavior of the system: the pressure drop scales quadratically with the flow rate, inversely with the square of the channel width, and linearly with the number of stages, while the dependence on the geometric ratio remains nonlinear through the parameter η.

For the structural condition for valve operation, the analytical model reveals that directional behavior only exists within a constrained region of the parameter space. The conditions required for rectification can be summarized as $ac \leq 1$, λ not excessively $N \leq N_{crit}$, $\theta \neq 0$. If any of these conditions is not accomplished, the angular interaction term vanishes and the diodicity approaches unity, $D \to 1$, indicating that the system no longer behaves as a functional Tesla valve.

4.3. Global Energetic Formulation

Combining all previous results, the final energetic expression for the reverse-flow pressure drop can be written as:

$$\Delta p_r = N\left[(K_c + K_{r0} + K_e) + \alpha\lambda^2\sin^2\theta\left(\frac{2-\sqrt{4-4ac}}{2a}\right)^2\right]\frac{\rho}{2}\left(\frac{Q}{S\cdot h}\right)^2, \tag{58}$$

with

$$a = (1 + \lambda\cos\theta) + \frac{N}{2}\alpha\lambda^2\sin^2\theta, \tag{59}$$

$$c = \frac{N}{2}(K_c + K_{r0} + K_e). \tag{60}$$

This expression represents the complete energetic closure of the model, explicitly showing how the pressure drop emerges from the interaction between inertial effects, geometric configuration, and nonlinear flow redistribution.

4.4. Maximum Projected Number of Stages

Considering that the existence condition is $\Delta = b^2 - 4ac \geq 0$ with $b = -2 \Rightarrow b^2 = 4$, then $\Delta = 4 - 4ac \geq 0 \Rightarrow ac \leq 1$. Using the definitions from Equation (42), the dominant contribution for large N is:

$$ac \approx \left(\frac{N}{2}\alpha\lambda^2\sin^2\theta\right)\left(\frac{N}{2}(K_c + K_{r0} + K_e)\right) \tag{61}$$

which simplifies to

$$ac \approx \frac{N^2}{4}\alpha\lambda^2\sin^2\theta(K_c + K_{r0} + K_e). \tag{62}$$

An upper bound for the number of diode stages can be obtained from the discriminant condition of the structural equation. For large values of N, the dominant contributions to the coefficients scale as $a \sim \frac{N}{2}\alpha\lambda^2\sin^2\theta$ and $c \sim \frac{N}{2}(K_c + K_{r0} + K_e)c$. Substituting these expressions into the existence condition $ac \leq 1$ yields:

$$\frac{N^2}{4}\alpha\lambda^2\sin^2\theta(K_c + K_{r0} + K_e) \leq 1 \tag{63}$$

Then,

$$N_{crit} \leq \frac{2}{\sqrt{\alpha\lambda^2\sin^2\theta(K_c + K_{r0} + K_e)}} \tag{64}$$

This expression defines an upper bound for the number of stages within which the analytical model admits real solutions for the flow-partition parameter. Beyond this limit, the mathematical structure of the model ceases to provide solutions under the assumptions employed.

4.5. Angular Condition and Analytical Range

The diodicity is given by:

$$D = 1 + \frac{\alpha\lambda^2 \sin^2\theta}{K_c + K_{r0} + K_e}\eta_r^2. \tag{65}$$

Differentiating with respect to the angle,

$$\frac{\partial D}{\partial \theta} \propto 2\sin\theta\cos\theta. \tag{66}$$

The mathematical maximum occurs at $\theta = 90^\circ$. However, this is a purely formal result. In real flows, such an angle induces strong separation, recirculation and additional losses not captured in the simplified model.

This system has a structural conflict due to having a high amount of θ. The greater the amount of θ, the more likely it is that the components of the system will have a good angular momentum transfer through their interaction. However, as θ increases, so do the irretrievable losses associated with the components of the system due to factors such as frictions, displacements, and turbulence. Therefore, the momentum transfer will eventually have an offset value from the efficiency losses as the irretrievable losses increase. Therefore, the most appropriate structure would be one that is sub-perpendicular, where angular momentum transfers at a reasonable value while still allowing for an adequate amount of energy to be lost. From the structural solution, the geometric constraint on the area ratio is $\eta \propto \frac{1}{\lambda^2}$.

Substituting into the diodicity expression leads to the limiting behaviors, $D \to 1$ as $\lambda \to \infty$ and $D \to 1$ as $\lambda \to 0$. This immediately rules out naive design intuition: neither very large nor very small area ratios produce rectification. Instead, the system admits an intermediate regime where angular interaction is maximized without suppressing the diverted flow.

4.6. Constraint on the Main Channel Width

Since $\lambda = \frac{S \cdot h}{A_r}$, an increase in the main channel width S produces a coupled set of hydrodynamic effects. First, the axial velocity decreases due to the enlargement of the cross-sectional flow area. Second, the diverted flow fraction η is reduced, as a wider channel weakens the mechanism that redirects the flow into lateral branches. Third, the angular dissipation term is nullified because the flow experiences less curvature-induced resistance.

As a direct consequence of these combined effects, the diodicity approaches unity for large values of S, $D \to 1$. This implies a strict design requirement: the main channel width cannot be arbitrarily increased. Instead, a finite value must be maintained and tightly controlled, since excessive widening suppresses the rectification effect and causes the system to behave as a passive symmetric duct.

The sensitivity with respect to the number of stages is indirect and mediated through the diverted flow fraction η. This relationship can be written as:

$$\frac{dD}{dN} = \frac{\partial D}{\partial \eta}\frac{d\eta}{dN} \tag{67}$$

For sufficiently large values of N, it follows that $\frac{d\eta}{dN} < 0$, which implies $\frac{dD}{dN} < 0$, beyond a certain threshold. This suggests a critical result: diodicity reaches a maximum before a critical number of stages N_{crit}. Adding more stages beyond that point degrades the rectification capability rather than improving it, due to accumulated losses and redistribution of the flow that diminish directional asymmetry.

For the system to behave as a functional Tesla valve, the following conditions must be simultaneously satisfied:

1. $ac \leq 1$,
2. $0 < \eta < 1$,
3. $N < N_{crit}$,
4. $\theta \neq 0$,
5. λ is finite.

Disagreement of any of these conditions leads to $D \to 1$ and the system degenerates into a passive duct with no directional behavior. The structural conditions of the model can be condensed into a compact design inequality:

$$\boxed{\alpha\lambda^2 \sin^2\theta (K_c + K_{r0} + K_e) N^2 \lesssim 4} \tag{68}$$

This expression defines the admissible design space by balancing geometric amplification effects with dissipative losses. In addition, the model suggests practical geometric bounds of approximately ($\theta \approx 60^\circ - 90^\circ$) and ($\lambda = O(1-10)$) These ranges should not be interpreted as strict physical limits, but rather as characteristic regions where the mechanisms responsible for flow rectification remain most effective within the assumptions of the present framework. For branch angles substantially larger than (90°), the diverted flow tends to align progressively with the main streamwise direction, reducing the effectiveness of lateral flow redistribution and the associated directional asymmetry. Consequently, although such geometries remain physically admissible, their contribution to rectification may become progressively less significant, causing the valve behavior to approach that of a conventional flow passage.

4.7. Final Structural Interpretation

The analytical structure of the model leads to a conclusion that directly challenges naive engineering intuition: the performance of a Tesla valve does not improve monotonically by simply increasing geometric or structural parameters. In particular, increasing the number of stages, widening the main channel, or enlarging the branch angle does not guarantee enhanced rectification. On the contrary, the governing equations reveal that such changes, beyond certain thresholds, actively degrade the mechanism responsible for directional behavior.

This non-monotonic response emerges from the presence of multiple, independent constraints embedded in the model. First, there exists a mathematical limit imposed by the condition $ac \leq 1$, which ensures the existence of real solutions for the flow-partition parameter η. Once this condition is violated, the model ceases to admit meaningful solutions, indicating that the assumed internal flow structure cannot be sustained. This is not a matter of physical failure of the device, but of mathematical inadmissibility within the reduced-order framework: the assumed flow-partition structure ceases to admit real-valued solutions under the adopted closure assumptions.

Second, a geometric constraint arises through the area ratio λ. The model shows that both extreme limits, $\lambda \to 0$ and $\lambda \to \infty$, lead to the same outcome: the suppression of diodicity. When λ is too small, the lateral branches become hydraulically irrelevant; when it is too large, the diverted flow fraction collapses due to the scaling $\eta \propto 1/\lambda^2$. In both cases, the angular interaction term vanishes, eliminating the asymmetry required for rectification.

Third, the system is subject to a cumulative constraint associated with the number of stages. While the total pressure drop increases linearly with N, the internal coupling through $\eta(N)$ introduces nonlinear feedback that limits performance. Within the assumptions of the present analytical formulation, the diodicity is predicted to decrease beyond

a critical number of stages N_{crit}. This proposes a clear upper bound: adding more stages eventually becomes counterproductive.

Finally, there is an energetic constraint linked to the angular dissipation mechanism. The term responsible for rectification, proportional to $\alpha(\eta\lambda)^2 sin^2\theta$, depends critically on maintaining a balance between flow diversion and geometric amplification. When this balance is disrupted (either by excessive channel width, unfavorable scaling of λ, or degradation of η), the angular contribution collapses, and the model predicts a reduction in directional behavior.

Taken together, these constraints define a bounded region in the parameter space within which rectification can exist. Outside this region, the Tesla valve does not gradually lose efficiency; it undergoes a qualitative transition. The diodicity approaches unity, and the system behaves as a passive duct with symmetric losses. In this sense, rectification is not an intrinsic property of the geometry alone, but an emergent phenomenon that arises only when strict structural, geometric, and energetic conditions are simultaneously satisfied.

4.8. Closure of Loss Coefficients from First Principles

The loss coefficients K_c, K_{r0}, and K_e are traditionally treated as empirical parameters. Within the present framework, however, they are interpreted through physics-based scaling arguments associated with momentum redistribution, flow separation, and viscous dissipation mechanisms. The following development should, therefore, be regarded as a physics-based scaling closure for the loss coefficients rather than a strict derivation from first principles. The objective is not to eliminate modeling assumptions, but to replace purely empirical constants with physically motivated closures that retain analytical tractability.

4.8.1. Contraction Loss Coefficient K_c

A geometric contraction in the flow passage induces a local acceleration of the fluid as it transitions from the upstream section toward the reduced area. This acceleration is not purely ideal, since, depending on the contraction ratio, the flow may undergo partial separation, leading to the formation of a likewise vena contraction downstream of the minimum geometric section. From a control volume perspective, the pressure drop associated with this process can be estimated by applying momentum conservation between the upstream section and the contraction region. Under this framework, the pressure loss due to contraction can be expressed as proportional to the square of the velocity difference between these two sections, leading to:

$$\Delta p_c \sim \frac{\rho}{2}(V_c - V_0)^2. \tag{69}$$

To express this relation in terms of geometric parameters, the velocities can be rewritten using the continuity equation. Assuming a constant volumetric flow rate, the velocities at the contraction and upstream section are given by $V_c = Q/A_c$ and $V_0 = Q/A_0$, respectively. Substituting these expressions into Equation (69) yields:

$$\Delta p_c \sim \frac{\rho}{2} Q^2 \left(\frac{1}{A_c} - \frac{1}{A_0}\right)^2. \tag{70}$$

This form makes explicit that the pressure loss is governed by the mismatch between inverse areas, highlighting the role of geometric contraction in amplifying velocity gradients.

For a more general and dimensionless characterization, the pressure drop is normalized by the upstream dynamic pressure $\frac{\rho V_0^2}{2}$, and we obtain:

$$K_c \sim \left(\frac{A_0}{A_c} - 1\right)^2. \tag{71}$$

At this point, it is convenient to introduce the contraction ratio as:

$$\beta = \frac{A_c}{A_0}, \tag{72}$$

which provides a compact measure of the geometric restriction. In terms of this parameter, the loss coefficient takes the form:

$$K_c \sim \left(\frac{1}{\beta} - 1\right)^2. \tag{73}$$

This final expression reveals a key scaling behavior: the contraction loss coefficient K_c is not arbitrary, but instead it scales with the square of the inverse area ratio. As a consequence, mild contractions ($\beta \approx 1$) produce relatively small penalties, whereas stronger contractions ($\beta \ll 1$) lead to a rapid and nonlinear increase in losses, reflecting the intensified acceleration and enhanced likelihood of flow separation.

4.8.2. Baseline Friction–Recirculation Term K_{r0}

This term represents distributed losses in the main path, including wall friction and mild recirculation. Starting from the Darcy–Weisbach formulation:

$$\Delta p_f = f \frac{L}{D_h} \frac{\rho V_0^2}{2}. \tag{74}$$

The baseline friction–recirculation term is expressed as:

$$K_{r0} = f \frac{L}{D_h}. \tag{75}$$

where f represents an effective friction factor. In the present formulation, which focuses on inertia-dominated flow conditions, f is treated as an effective constant parameter that accounts for the combined contribution of viscous dissipation and turbulence-induced mixing. This assumption ensures consistency with the quadratic scaling of pressure losses adopted throughout the model. The explicit dependence of f on the Reynolds number can be incorporated as an extension of the present formulation but is not considered in the base model.

4.8.3. Expansion Loss Coefficient K_e

The expansion process is fundamentally governed by flow separation and subsequent turbulent mixing as the fluid transitions from a smaller cross-sectional area to a larger one. Unlike contractions, where acceleration dominates, expansions are characterized by a deceleration that is typically accompanied by boundary layer detachment and the formation of recirculation zones. These phenomena introduce irreversible losses that are primarily associated with momentum redistribution and mixing. From an energy perspective, the pressure loss across the expansion can be estimated based on the mismatch between the upstream and downstream velocities. This leads to the classical scaling:

$$\Delta p_e \sim \frac{\rho}{2}(V_1 - V_2)^2 \tag{76}$$

To relate this expression to the geometry of the system, the velocities are rewritten using continuity. For a constant volumetric flow rate, the velocities in the upstream and downstream sections are given by:

$$V_1 = \frac{Q}{A_1}, \tag{77}$$

$$V_2 = \frac{Q}{A_2}. \tag{78}$$

Substituting these relations into the previous expression and normalizing by the upstream dynamic pressure leads to a dimensionless characterization of the losses through the expansion loss coefficient,

$$K_e \sim \left(1 - \frac{A_1}{A_2}\right)^2. \tag{79}$$

In order to express this dependence in a more compact and transparent form, the expansion ratio is introduced as:

$$\gamma = \frac{A_1}{A_2} \tag{80}$$

which allows the loss coefficient to be written as:

$$K_e \sim (1 - \gamma)^2 \tag{81}$$

This formulation highlights that the losses are governed by the square of the velocity mismatch induced by the area change. Consequently, the dominant mechanism is not merely geometric expansion, but the irreversible mixing process required to redistribute momentum between regions of differing velocities. As a result, even moderate expansions can generate significant losses if they promote strong separation and mixing, emphasizing that the dissipation is intrinsically linked to the breakdown of ordered kinetic energy into turbulent fluctuations rather than to geometry alone.

4.8.4. Unified Structural Form

The next step consists of reinserting the previously derived scaling relations into the global model, thereby replacing empirical closures with grounded expressions. In particular, each contribution to the total loss is associated with a distinct mechanism: geometric acceleration in contractions, viscous dissipation along the flow path, and irreversible mixing during expansion. The contraction loss coefficient is expressed in terms of the contraction ratio β as:

$$K_c \sim \left(\frac{1}{\beta} - 1\right)^2, \tag{82}$$

which captures the effect of flow acceleration and the potential onset of separation at the contraction.

The frictional contribution along the channel is described through the classical scaling:

$$K_{r0} \sim f\frac{L}{D_h}, \tag{83}$$

where f represents the friction factor, L the characteristic length of the flow path, and D_h the hydraulic diameter, thus accounting for viscous dissipation distributed along the walls.

Finally, the expansion loss coefficient, governed by velocity redistribution and turbulent mixing, is given by:

$$K_e \sim (1 - \gamma)^2, \tag{84}$$

where γ denotes the expansion ratio. By combining these three contributions, the total baseline loss coefficient can be written as:

$$K_{base} = \left(\frac{1}{\beta} - 1\right)^2 + f\frac{L}{D_h} + (1-\gamma)^2 \tag{85}$$

This expression replaces three empirical constants with three interpretable mechanisms. Specifically, the first term represents geometric acceleration associated with contraction, the second term accounts for viscous dissipation due to wall friction, and the third term quantifies the irreversibility introduced by mixing processes in the expansion. In this way, the model acquires a clearer physical structure, where each contribution can be independently analyzed and related to measurable geometric and flow parameters, rather than relying on purely empirical adjustments.

4.9. Impact on the Global Model

Substituting the baseline loss formulation into the expression for diodicity yields:

$$D = 1 + \frac{\alpha\lambda^2 \sin^2\theta}{K_{base}}\eta^2 \tag{86}$$

where K_{base} is now explicitly defined in terms of contraction, friction, and expansion mechanisms. This substitution closes the model by expressing the rectification performance as a balance between geometric forcing, embedded in the numerator, and dissipative effects, contained in the denominator.

In this form, the structure of the model reveals several important features. First, the dependence on geometry is entirely captured through dimensionless ratios, such as β, γ, λ, and the angular parameter θ. This implies that the formulation is scale-independent and can be applied across different sizes provided that geometric similarity is preserved.

Second, the influence of the Re is not introduced explicitly, but rather embedded through the friction factor f, which appears in the definition of K_{base}. As a consequence, the model retains sensitivity to the flow regime, laminar, transitional, or turbulent, without requiring an explicit Re in the governing equation.

Finally, despite incorporating multiple physical mechanisms, the model remains fully analytical. All contributions are expressed through closed-form relationships, which allows direct evaluation and facilitates parametric analysis without the need for numerical closure. This analytical character is particularly advantageous for design purposes, as it enables rapid exploration of the influence of geometry and flow conditions on diodicity while preserving a clear physical interpretation of each term.

5. Results and Validation

The validation of the analytical model proposed in this work to describe the relationship between volumetric flow rate and pressure drop in Tesla valves faces an inherent limitation due to the absence of experimental or numerical datasets. Most of the available studies focus on performance metrics for specific geometries, such as heat transfer enhancement or flow rectification efficiency, rather than on the formulation or verification of an analytical expression governing the hydrodynamic behavior of these systems under liquid flow conditions. Consequently, the validation framework adopted herein is based on internal consistency, asymptotic correctness, parametric sensitivity, and agreement with established qualitative trends rather than direct comparison with external datasets.

A first level of validation is provided by the consistency of the model with the fundamental principles of fluid mechanics. As illustrated in Figure 2, pressure losses increase

as inertial effects become progressively dominant, reproducing the expected Reynolds-dependent increase in hydraulic resistance.

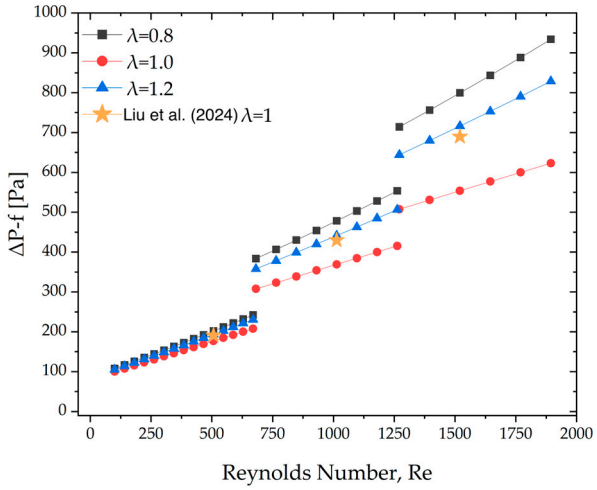


Figure 2. Pressure losses increase with inertial dominance. The trend reflects Reynolds-dependent hydraulic resistance; here, the area ratio is $\lambda = A_0/A_r$ [15].

The resulting formulation predicts a quadratic dependence of pressure drop on volumetric flow rate, $\Delta p \propto Q^2$, which is characteristic of inertia-dominated internal flows. This behavior is explicitly verified through numerical evaluation of the model, where a quadratic fit of the computed pressure drop as a function of flow rate confirms the expected scaling. As shown in Figure 3, the computed pressure drop follows a nearly linear trend when represented against Q^2, confirming the inertia-dominated scaling predicted by the analytical formulation. At the same time, viscous effects are incorporated through the Reynolds-number-dependent friction term, ensuring that the model captures the influence of fluid properties and flow regime. Although the formulation does not explicitly resolve transitional flow physics, it provides a consistent representation of the interplay between inertial and viscous effects.

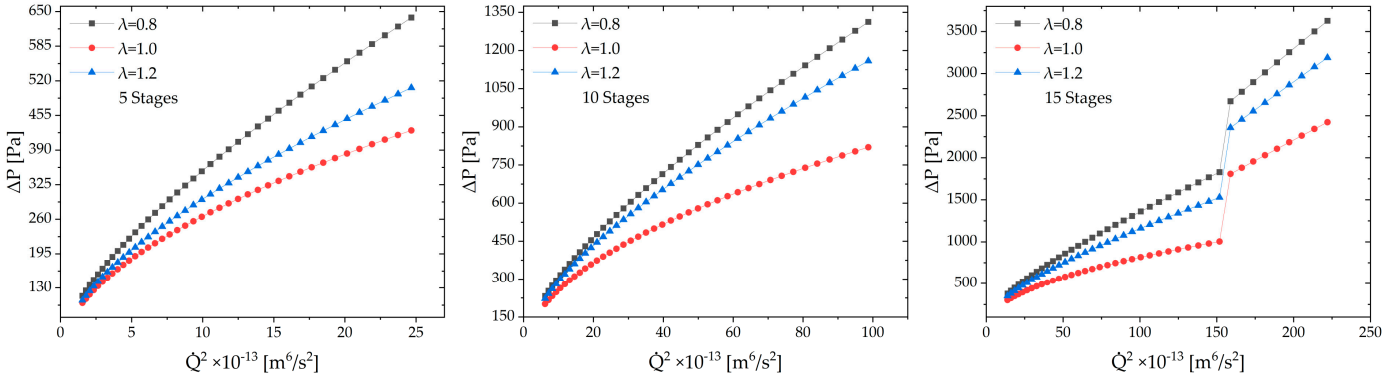


Figure 3. Linear trend indicates $\Delta p \propto Q^2$. Quadratic trend confirms inertia-dominated losses. Deviations reflect geometric coupling and non-hydraulic effects.

A second level of validation is associated with the model's ability to reproduce directional asymmetry, which is the defining operational characteristic of Tesla valves. The analytical formulation predicts an increase in effective hydraulic resistance under reverse-flow conditions due to the activation of angular dissipation terms, while maintaining lower resistance in the forward direction. This behavior is consistent with widely reported qualitative observations in Tesla-type geometries, where flow redirection and momentum exchange lead to asymmetric energy dissipation [15]. This behavior is consistent with

experimental observations reported by Nguyen et al. [6], who showed that Tesla valves develop significantly larger hydraulic resistance under reverse-flow conditions, leading to measurable diodicity at sufficiently high Reynolds numbers. Rather than resolving detailed vortex dynamics, the model provides an interpretable parametric representation of this asymmetry through its dependence on geometric and flow-partition parameters.

The resulting directional asymmetry is quantified in Figure 4 through the diodicity ratio, where values greater than unity indicate the emergence of asymmetric hydraulic resistance between forward- and reverse-flow directions.

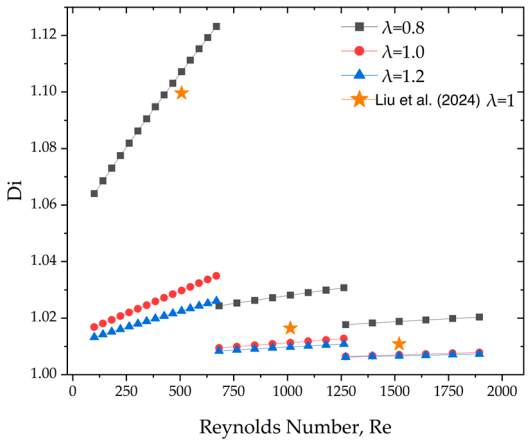


Figure 4. Diodicity = $\Delta P - r/\Delta P - f$. Values > 1 indicate directional hydraulic asymmetry (diode effect behavior) induced by nonlinear coupling between forward and reverse flow [15].

The influence of geometric complexity constitutes a third validation axis. The model predicts that the total pressure losses increase with the number of stages, while the diodicity exhibits a nonlinear dependence mediated by the flow-partition parameter. This result is consistent with the known behavior of Tesla valves, where increasing the number of stages enhances resistance but does not necessarily improve rectification efficiency proportionally. Additional support for the analytical trends predicted by the model can be found in previously reported numerical investigations of Tesla valves.

The predicted sensitivity to geometric parameters is consistent with studies showing that modifications in channel geometry significantly alter the pressure-drop asymmetry between forward- and reverse-flow directions [31]. Similar stage-dependent trends have also been reported, where the accumulation of successive flow redirections increases reverse-flow losses more rapidly than forward-flow losses [32]. Furthermore, the dependence on the area ratio and channel dimensions reflects the well-established sensitivity of Tesla valve performance to geometric configuration, particularly regarding the redistribution of flow between the main channel and lateral branches. Recent numerical studies further confirm that the geometric configuration of bifurcated channels strongly influences diodicity and pressure-loss asymmetry [23]. These observations collectively support the qualitative trends predicted by the present analytical formulation.

A key validation element arises from the intrinsic admissibility condition of the model, defined by the inequality $ac \leq 1$, which bounds the existence of meaningful solutions to the nonlinear governing equation. This condition emerges directly from the analytical structure and is verified numerically through two-dimensional parameter maps in the (θ, N) space for different geometric configurations. The identification of this admissible domain provides a rigorous constraint on the applicability of the model and prevents non-physical predictions outside its range of validity.

Additionally, solutions of the nonlinear equation are retained by enforcing the constraint $0 < \eta < 1$, ensuring consistency with the definition of the flow-partition parameter.

This filtering step guarantees that the numerical evaluation remains within the interpretable solution branch.

Further validation is obtained through asymptotic analysis. In the low-Reynolds-number limit, viscous effects dominate and the formulation reduces to a friction-controlled regime consistent with classical laminar flow behavior. Conversely, in the high-Reynolds-number limit, inertial contributions prevail and the quadratic dependence on flow rate becomes dominant. In geometric limits, the model also behaves consistently: as the number of stages approaches zero, the system degenerates into a straight channel with negligible directional effects, while extreme geometric configurations suppress angular interaction terms, leading to a diodicity approaching unity. These asymptotic behaviors confirm that the model remains well-posed and consistent across its admissible parameter space. This inertial behavior is further supported by Figure 5, where the ratio $\Delta P/Q^2$ remains approximately constant as the number of stages increases, consistent with an inertia-dominated regime.

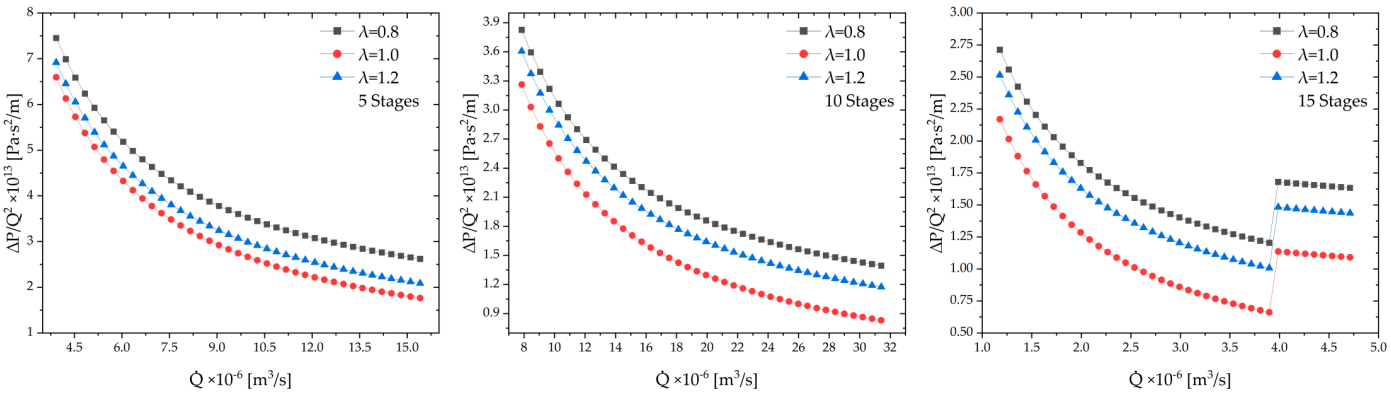


Figure 5. Inertial regime check by stages. Constant $\Delta P/Q^2$ ratio indicates pure inertial regime. Deviations indicate viscous or transitional effects or nonlinear coupling effects.

Dimensional consistency provides an additional layer of validation. All terms in the governing formulation can be expressed in a dimensionless framework, ensuring that the predicted behavior depends solely on nondimensional groups rather than arbitrary unit choices. Moreover, the structure of the model does not exhibit singularities or divergences within the admissible domain defined by the discriminant condition, further supporting its robustness. The evolution of the admissibility parameter is presented in Figure 6, where the condition ac = 1 defines the analytical admissibility boundary separating admissible and non-admissible regions of the formulation.

Overall, the combination of internal consistency, asymptotic correctness, parametric sensitivity analysis (presented in Appendix A), and the identification of a well-defined admissible solution domain constitutes a consistency-based validation framework for assessing the internal coherence and applicability range of the proposed analytical formulation.

Although a formal sensitivity analysis of the loss coefficients lies beyond the scope of the present work, the structure of the governing equations indicates that K_c, K_{r0}, K_e and the geometric ratio λ are the dominant parameters controlling diodicity, while Reynolds number dependence enters through the friction factor f in K_{base} rather than through structural modification of the solution form. A systematic parametric sensitivity study is identified as a direct and tractable extension of the present framework.

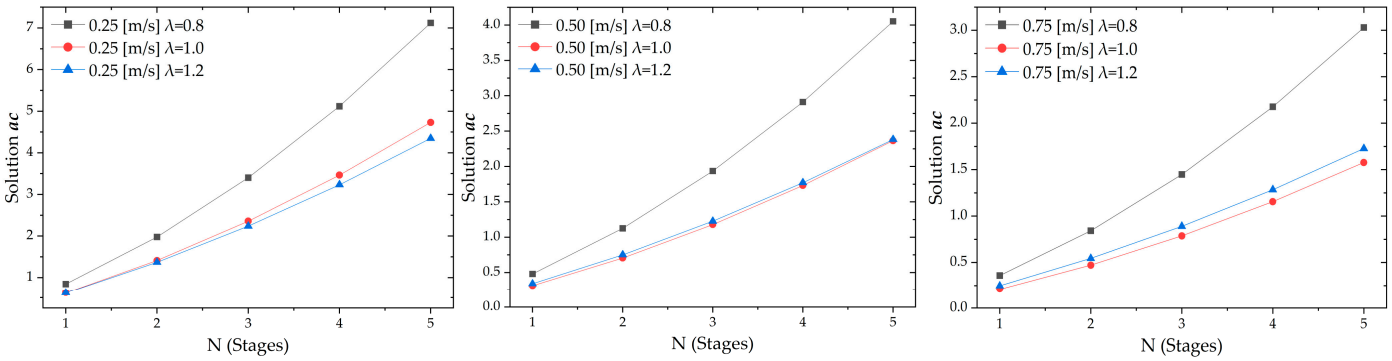


Figure 6. ac solution vs. total stages. ac defines the mathematical existence of real solution in the model formulation. $ac = 1$ indicates stability boundary or critical condition. $ac < 1$ indicates physical solution existence. $ac > 1$ indicates that the model becomes invalid (no real solution).

6. Analysis and Discussion

The hydrodynamic behavior of Tesla valves emerges from the coupled interaction between inertia, viscous dissipation, and geometric flow redistribution. Rather than treating these mechanisms independently, the present formulation incorporates them into a single nonlinear framework through the flow-partition parameter, η, which represents the fraction of flow diverted from the main channel into secondary branches. This interpretation provides a physically meaningful description of rectification, where directional behavior is not imposed through empirical assumptions but emerges from the interaction between flow redistribution and energy dissipation.

A distinctive aspect of the proposed formulation is that η is not prescribed a priori nor introduced as a fitting parameter. Instead, it is obtained as the solution of a nonlinear balance involving inertial forcing, hydraulic losses, and geometric forcing terms. Its value emerges from the governing equation and is constrained by the admissibility condition $0 < \eta < 1$, ensuring that only physically interpretable flow partitions are retained. Consequently, the directional response of the valve becomes an emergent property of the governing equation itself rather than an imposed assumption. In this sense, diodicity should not be interpreted exclusively as a consequence of geometric asymmetry, but rather as the macroscopic manifestation of how geometry modifies the partition of flow and the associated dissipation mechanisms. The analytical structure, therefore, suggests that geometric asymmetry alone is insufficient to explain rectification unless it is coupled with an effective redistribution of momentum and energy within the device.

The resulting equation reveals that the hydraulic response of the valve is controlled by the competition between two opposing tendencies. On one hand, inertial effects promote flow penetration into secondary paths, increasing the possibility of momentum redistribution and directional asymmetry. On the other hand, hydraulic losses oppose this redistribution through frictional and local dissipation mechanisms. The flow-partition parameter emerges from the equilibrium between these competing effects, providing a direct link between geometry, operating conditions, and hydraulic performance. This interpretation gives physical meaning to the nonlinear structure of the governing equation and explains why rectification cannot be described solely through pressure-drop correlations or purely geometric arguments.

The formulation further indicates that the effective hydraulic resistance contains two distinct contributions: a baseline resistance associated with conventional hydraulic losses and an additional angular dissipation term associated with flow redirection. The latter becomes increasingly important as the flow is forced to deviate from the main channel, thereby enhancing energy dissipation and directional asymmetry. Within the

framework of the model, forward flow corresponds to configurations where this additional contribution remains limited, whereas reverse flow activates stronger angular dissipation. As a consequence, the difference between forward and reverse pressure losses emerges naturally from the analytical structure without requiring separate empirical formulations for each direction.

Although the present model does not explicitly resolve local vortex dynamics, flow separation, shear-layer development, or transient recirculation structures, these processes remain indirectly represented through the scaling of the loss coefficients and their dependence on the Reynolds number and geometry. The formulation should, therefore, be interpreted as a reduced-order representation of the cumulative hydrodynamic effects generated by such mechanisms rather than as a direct description of the underlying flow field. This distinction is particularly important because the objective of the model is not to reproduce detailed fluid-dynamic structures but to identify the dominant parameters governing directional hydraulic behavior.

One of the most significant outcomes of the formulation is the emergence of the admissibility condition $ac \leq 1$, obtained directly from the nonlinear structure of the governing equation. This condition defines the region of parameter space in which real and physically interpretable solutions for η exist and was explored numerically through the two-dimensional maps presented in the Results Section. Outside this domain, no real and consistent value of η satisfies the governing equation, indicating that the assumed redistribution mechanism is no longer compatible with the constraints imposed by the analytical model. This condition does not represent a physical failure of the valve nor a hydrodynamic instability. Rather, it establishes a mathematical boundary defining the range of self-consistent solutions admitted by the formulation. The existence of this bounded admissible domain demonstrates that geometric forcing, hydraulic dissipation, and flow redistribution cannot vary independently but remain constrained by a nonlinear coupling that limits the feasible operating space predicted by the model.

This result suggests an alternative interpretation of Tesla valve operation. Instead of viewing performance as a quantity that can be indefinitely improved through geometric modification, the formulation predicts the existence of intrinsic constraints arising from the internal balance of the system. The appearance of a bounded admissible region suggests that increasing geometric complexity does not necessarily translate into improved rectification and may eventually reduce the effectiveness of the flow redistribution mechanism. Within the assumptions of the model, this behavior explains the emergence of a critical stage number, N_{crit}, and the existence of geometric configurations that become progressively less effective despite increasing structural complexity.

The role of the Reynolds number is particularly important because it governs the relative contribution of viscous and inertial effects. Through the Reynolds-dependent friction factor, the formulation incorporates the influence of fluid properties, characteristic dimensions, and flow velocity. At low Reynolds numbers, viscous dissipation dominates and limits flow redistribution, leading to weaker directional effects. As the Reynolds number increases, inertial contributions become progressively more important and the pressure drop approaches the characteristic quadratic scaling $\Delta P \propto Q^2$ observed in inertia-dominated internal flows. Consequently, the model predicts a gradual transition from friction-controlled behavior toward inertia-controlled behavior while preserving the same governing mathematical structure. For sufficiently high Reynolds numbers within the inertial regime considered in this work, inertial contributions become dominant and the formulation approaches the asymptotic scaling $\Delta P \propto Q^2$ obtained from the governing equations and evaluated numerically within the analytical framework. Under these conditions,

the hydraulic response is primarily controlled by momentum redistribution and geometric forcing, whereas viscous effects progressively lose influence on the overall pressure losses.

The geometric parameters of the valve influence this balance through complementary mechanisms. The branch angle controls the intensity of flow redirection and, therefore, the magnitude of the angular dissipation term. The area ratio governs the fraction of flow capable of entering secondary branches and directly affects the redistribution process represented by η. The number of stages acts as an accumulation mechanism that amplifies total losses while simultaneously modifying the nonlinear balance controlling flow partition. The formulation, therefore, predicts that the Reynolds number, geometry, and stage number cannot be optimized independently, since each parameter influences the same underlying redistribution–dissipation equilibrium.

From an engineering perspective, these results suggest that effective Tesla valve design should not focus exclusively on maximizing geometric asymmetry or increasing the number of stages. Instead, performance emerges from a balance between flow diversion, hydraulic losses, and inertial transport. The existence of the conditions $0 < \eta < 1$ and $ac \leq 1$ further indicates that feasible operating states are bounded by both physical and mathematical constraints. The model, therefore, provides a framework for identifying regions of parameter space where directional behavior is enhanced while maintaining consistency with the governing analytical assumptions. In this sense, the formulation may be interpreted as a design-oriented analytical tool capable of revealing dominant trends and admissible operating conditions before undertaking more detailed numerical or experimental investigations.

Finally, the proposed formulation provides a bridge between local hydrodynamic processes and global system-level behavior. While detailed fluid-dynamic phenomena occur at scales associated with flow separation, recirculation, and momentum exchange, their cumulative influence is incorporated into a reduced set of physically interpretable parameters. The resulting framework does not replace high-fidelity simulations or experiments, but offers a coherent analytical description that connects geometry, operating conditions, hydraulic losses, and directional behavior within a single mathematical structure. The central outcome of the present work is, therefore, not merely a pressure-drop correlation, but the identification of flow partition as a key governing variable within the present analytical framework through which the coupled effects of inertia, dissipation, and geometry determine Tesla valve rectification.

7. Conclusions

This work developed an analytical formulation for describing the hydrodynamic behavior of Tesla valves by relating pressure drop, flow partition, and directional resistance to the main geometric and hydraulic parameters of the system. The proposed model provides a reduced-order representation of the valve response based on interpretable quantities, including the flow-partition parameter, the area ratio between the main channel and lateral branches, the branch inclination angle, the number of stages, and the effective loss coefficients. The present formulation neglects transient vortex dynamics, three-dimensional effects, turbulence closures, wall roughness and inter-stage hydrodynamic memory effects. Consequently, the model should be interpreted as an analytical scaling framework intended to identify dominant trends and admissible operating regions.

The formulation reproduces the expected quadratic dependence between pressure drop and volumetric flow rate under inertia-dominated conditions, while also incorporating viscous effects through the effective friction contribution. In this way, the model captures the transition from baseline hydraulic resistance to directional amplification without requiring full resolution of the internal flow field.

A central outcome of the analysis is the identification of an admissible operating domain for the valve. The discriminant condition of the governing structural equation imposes a mathematical constraint on the existence of solutions for the flow-partition parameter. This result provides a theoretical criterion for distinguishing between feasible configurations and parameter combinations that fall outside the range of validity of the reduced-order formulation.

For practical design use, this admissibility condition is expressed through the compact inequality $\alpha\lambda^2\sin^2\theta\cdot(K_c + K_{r0} + K - e)\cdot N^2 \lesssim 4$ [Equation (68)], which couples geometric and hydraulic-loss parameters into a single first-order design criterion. This expression identifies the admissible region for effective rectification and provides a direct guideline for parameter selection prior to detailed simulation or fabrication.

The model also shows that Tesla valve performance is intrinsically non-monotonic with respect to geometric complexity. Increasing the number of stages, modifying the area ratio, or increasing the branch angle does not necessarily enhance rectification. Instead, effective directional behavior emerges only when flow diversion, angular interaction, and dissipative losses remain properly balanced. This finding indicates a rational basis for defining design limits and avoiding configurations that may increase total pressure losses without improving diodicity.

Another relevant contribution of the formulation is that it provides a consistent framework for interpreting diodicity as an emergent property of the coupled interaction between geometry and flow redistribution. The directional response is not treated as an empirical outcome alone, but as the result of identifiable hydraulic mechanisms represented through closed-form relationships. This makes the model useful for preliminary design, sensitivity analysis, and comparison among different Tesla valve configurations.

From an engineering perspective, one of the main contributions of the proposed formulation is its ability to reinterpret the Tesla valve as a parametrically tunable hydraulic component, by making explicit the analytical dependence of its rectifying behavior on a small set of governing parameters. The model identifies the critical variables that govern valve performance, including the number of stages, the area ratio between the main conduit and the lateral branches, the branch inclination angle, the flow-partition parameter, and the effective loss coefficients. This provides a practical framework for constraining the design space and for determining which parameters must be controlled during numerical simulations, laboratory experiments, and potential field-scale implementation. The study shows that there is no direct relationship between increased geometric complexity and rectification performance. Instead, the effective operation of a valve exists in a limited portion of the parameter space combinations where proper balances exist between flow splitting, angular momentum exchange and dissipative loss. This insight is particularly valuable for the design of Tesla-type devices in hydraulic engineering applications, including open-channel systems, where passive flow-control structures could be used to reduce backflow, regulate preferential flow paths, or enhance the resilience of drainage and flood-control infrastructure. Thus, beyond its theoretical relevance, the proposed model offers a practical basis for guiding the design, optimization, and scaling of Tesla valves from numerical prototypes to real hydraulic systems.

Author Contributions: Conceptualization, M.D.l.C.-Á. and R.B.; methodology, M.D.l.C.-Á., M.I.E.-D., F.J.C.G. and R.B.; software, M.D.l.C.-Á.; validation, M.D.l.C.-Á., M.I.E.-D. and F.J.C.G.; formal analysis, M.D.l.C.-Á. and M.I.E.-D.; investigation, M.D.l.C.-Á., M.I.E.-D., F.J.C.G. and R.B.; resources, M.D.l.C.-Á. and R.B.; data curation, M.D.l.C.-Á., M.I.E.-D. and F.J.C.G.; writing—original draft preparation, M.D.l.C.-Á., M.I.E.-D., F.J.C.G. and R.B.; writing—review and editing, M.D.l.C.-Á., M.I.E.-D., F.J.C.G. and R.B.; visualization, M.D.l.C.-Á.; supervision, R.B.; project administration, R.B. All authors have read and agreed to the published version of the manuscript.

Funding: This research received no external funding.

Data Availability Statement: The original contributions presented in the study are included in the article. Further inquiries can be directed to the corresponding author.

Acknowledgments: The authors gratefully acknowledge Tecnologico de Monterrey for its support and for providing the facilities and conditions necessary to carry out this research.

Conflicts of Interest: The authors declare that they have no known competing financial interests or personal relationships that could have appeared to influence the work reported in this paper.

Abbreviations

The following abbreviations are used in this manuscript:

Symbol	Definition	Units
S	Main channel width	m
h	Effective channel depth (hydraulic depth)	m
A_0	Cross-sectional area of the main channel	m^2
A_r	Cross-sectional area of the lateral branch	m^2
D_h	Hydraulic diameter of the main channel	m
P	Wetted perimeter	m
θ	Angle between main channel and branch axis	rad
L_r	Effective branch length	m
L_s	Axial spacing between consecutive Tesla stages	m
L_d	Hydrodynamic development length	m
$S_{(crit)}$	Critical channel width for rectification	m
Q	Total volumetric flow rate	m^3/s
Q_m	Flow remaining in the main channel	m^3/s
Q_r	Flow entering the branch	m^3/s
$\dot{m}$	Total mass flow rate	kg/s
$\dot{m}_m$	Mass flow rate in main channel	kg/s
$\dot{m}_r$	Mass flow rate in branch	kg/s
η	Flow-partition parameter, Q_r/Q	–
η_f	Flow-partition parameter in forward direction	–
η_r	Flow-partition parameter in reverse direction	–
$\eta_{(crit)}$	Critical flow-partition parameter	–
λ	Area ratio, A_0/A_r	–
V_0	Mean axial velocity in the main channel	m/s
V_r	Mean velocity in the branch	m/s
V_x	Axial velocity component	m/s
V	Velocity vector	m/s
ρ	Fluid density	kg/m^3
μ	Dynamic viscosity	Pa·s
ν	Kinematic viscosity (μ/ρ)	m^2/s
g	Gravitational acceleration	m/s^2
p	Static pressure	Pa
Δp	Pressure drop	Pa
Δp_{et}	Pressure drop per Tesla stage	Pa
ΔpN	Total pressure drop for N stages	Pa
Δp_f	Total pressure drop in forward flow	Pa
Δp_r	Total pressure drop in reverse flow	Pa
$\Delta p_{(r-f)}$	Reverse-forward pressure difference	Pa

F_x	Net axial force	N
F	Total force vector acting on the control volume	N
A_s	Control surface area	m^2
N	Unit outward normal vector	–
M_x	Axial momentum flux	N
A_s	Control surface area	m^2
N	Unit outward normal vector	–
M_x	Axial momentum flux	N
Re	Reynolds number, $\rho V_0 D_h/\mu$	–
Φ	Dimensionless pressure parameter	–
ΦN	Dimensionless pressure parameter including N stages	–
D	Hydraulic diodicity coefficient	–
D(N)	Diodicity as a function of stage number	–
K_c	Contraction loss coefficient	–
K_{r0}	Base recirculation loss coefficient	–
K_e	Expansion loss coefficient	–
K_{impact}	Angular impact loss coefficient	–
K_c'	Effective contraction loss coefficient in reverse flow	–
K_e'	Effective expansion loss coefficient in reverse flow	–
$K_{r0,r}$	Reverse-flow recirculation coefficient	–
A	Angular momentum interaction coefficient	–
ΣK	Total hydraulic loss coefficient	–
ΣK_{et}	Total loss coefficient per Tesla stage	–
$\Sigma K_{et,f}$	Stage loss coefficient in forward flow	–
$\Sigma K_{et,r}$	Stage loss coefficient in reverse flow	–
ΣK_f	Total loss coefficient in forward flow	–
ΣK_r	Total loss coefficient in reverse flow	–
ΣK_{tot}	Overall hydraulic loss coefficient of the valve	–
N	Number of Tesla stages	–
N/2	Structural accumulation factor appearing in the governing equation	–
N_{crit}	Critical number of stages predicted by the model	–
A	Quadratic coefficient of the structural equation	–
B	Linear coefficient of the structural equation	–
C	Constant coefficient of the structural equation	–
Δ	Discriminant of the structural equation	–
$\sqrt{\Delta}$	Real-solution existence term	–
ac	Structural stability product	–
dD/dN	Sensitivity of diodicity to stage number	–
$d\eta/dN$	Sensitivity of flow partition to stage number	–
$\partial D/\partial\theta$	Angular sensitivity of diodicity	rad^{-1}
$V_0 = Q/A_0$	Mean axial velocity	
$V_r = Q_r/A_r$	Mean branch velocity	
$Q = Q_m + Q_r$	Conservation of mass	
$\eta = Q_r/Q$	Flow-partition parameter	
$\lambda = A_0/A_r$	Geometric area ratio	

$\Delta p = \Sigma K(\rho V_0^2/2)$	Hydraulic loss formulation
$\Phi = (A_0^2/\rho Q^2)\Delta p$	Dimensionless pressure parameter
$(1 + \lambda\cos\theta)\eta^2 - 2\eta + \Phi = 0$	Structural equation
$\Phi_N = N\Sigma K_{et}/2$	Multi-stage coupling parameter
$D = \Sigma K_r/\Sigma K_f$	Diodicity definition
$Re \propto Q$	Reynolds number scaling
$\Delta p \propto Q^2$	Inertial pressure-loss scaling
$\lambda \propto S$	Area-ratio geometric scaling
$V_0 \propto 1/S$	Velocity dilution with width
$\Delta pr - \Delta p_f \propto NQ^2$	Accumulated rectification effect
$\eta \propto 1/\lambda^2$	Large-area-ratio asymptotic limit
$D \to 1$ as $\lambda \to 0$	Loss of rectification
$D \to 1$ as $\lambda \to \infty$	Loss of rectification
$N \leq N_{crit}$	Structural validity condition
$ac \leq 1$	Real-solution existence condition

Appendix A. Sensitivity Analysis of the Reduced-Order Formulation

This appendix presents a sensitivity analysis of the proposed analytical formulation, intended to identify, in quantitative terms, which parameters control the admissibility parameter ac and the diodicity Di within the present model. The analysis is organized into a local component, based on normalized partial derivatives evaluated at the nominal operating point, and a global component, based on one-at-a-time parameter sweeps and two-dimensional admissibility maps. The nominal operating point corresponds to the conditions reported in the main text ($V = 0.25$ m/s, $Dh = 0.002$ m, $\rho = 1000$ kg/m^3, $\mu = 0.001$ Pa·s, $\theta = 45°$), for which $Re = 5.00 \times 10^2$ (laminar regime) and $Kbase = Kc + Kr0 + Ke = 0.640$ for $\lambda = 1.0$. Under these conditions, the discriminant condition $ac \leq 1$ is satisfied only for $N = 1$, since ac already exceeds unity for $N \geq 2$; this is the same boundary that produces the rapid growth of the ac curves reported in Figure 6 of the main text. The nominal point $N = 1$ is, therefore, adopted as the local-sensitivity evaluation point, while the global sweeps below extend the stage count up to $N = 20$ in order to expose the full admissible-to-inadmissible transition.

Appendix A.1. Local Sensitivity (Normalized Elasticities)

For each governing parameter $pi \in N, \lambda, \theta, K_{base}$, a normalized sensitivity coefficient, or elasticity, is defined as

$$Si = (\partial Y/\partial pi)\cdot(pi/Y), \tag{A1}$$

where Y denotes one of the model outputs (ac or Di) and the partial derivative is estimated through a central finite-difference scheme with a relative perturbation of 0.1% around the nominal value of pi, with all remaining parameters being held fixed. Because Si is dimensionless, it allows a direct comparison between parameters of different physical nature and units, such as a geometric ratio, an angle, an integer stage count, and a composite loss coefficient. The resulting elasticities, evaluated at the nominal point ($\lambda = 1.0$, $\theta = 45°$, $N = 1$, $K_{base} = 0.640$), are summarized graphically in Figure A1.

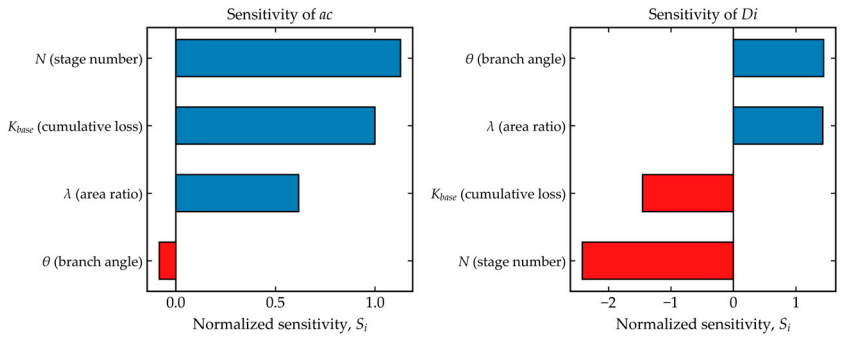


Figure A1. Normalized local sensitivity (elasticity) of the admissibility parameter ac (**left**) and the diodicity Di (**right**) with respect to the stage number N, the cumulative loss coefficient K_{base}, the area ratio λ, and the branch angle θ, evaluated at the nominal operating point. Blue bars indicate a positive elasticity (the output increases with the parameter); red bars indicate a negative elasticity.

The results in Figure A1 show that the stage number N ($S = 1.13$) and the cumulative loss coefficient K_{base} ($S = 1.00$) are the dominant parameters controlling the admissibility parameter ac, followed by the area ratio λ ($S = 0.62$), while the branch angle θ exhibits a comparatively small elasticity ($S = -0.08$). This hierarchy is consistent with the structural form of the coefficients a and c in Equation (43): since c scales linearly with N and with K_{base}, and a is dominated, for moderate λ, by the geometric term $1 + \lambda\cos\theta$ rather than by the angular-interaction term, the product ac responds most strongly to N and to the cumulative losses, while θ enters mainly through the bounded factor $\sin^2\theta$, whose derivative is small in the vicinity of 45°. Conversely, for the diodicity Di, the ranking is reversed: θ ($S = 1.45$) and λ ($S = 1.43$) emerge as the dominant parameters, while K_{base} ($S = -1.46$) and N ($S = -2.42$) act with negative elasticity. This sign reversal follows directly from the definition of Di in Equation (65): because Di depends on λ and θ both directly, through the angular-interaction term $\alpha\lambda^2\sin^2\theta \cdot K_{base}$, and indirectly, through η, which itself decreases as N or K_{base} increase, the net effect on Di of increasing N or K_{base} is dominated by the $1/\eta^2$ term and, therefore, reduces Di, whereas an increase in λ or θ strengthens the angular-interaction numerator faster than it depletes η. Taken together, these results indicate that N and K_{base} are the parameters that primarily govern whether the formulation remains within its admissible domain, while λ and θ are the parameters that primarily govern the magnitude of the rectification effect once admissibility is satisfied. This separation of roles is consistent with the distinction, established in the main text, between the discriminant condition $ac \leq 1$ as a mathematical admissibility constraint and the diodicity Di as the physically interpretable output of the model.

As a complementary verification, a Monte Carlo sampling of the admissible parameter space (8×10^6 realizations) was performed, and Spearman rank correlations between the input parameters and the diodicity output were computed. The analysis confirms the dominant influence of λ ($\rho_S = 0.60$) on Di, consistent with the local elasticity results reported above.

Appendix A.2. Global Sensitivity: One-at-a-Time Parameter Sweeps

The local elasticities reported above are strictly valid only in the immediate neighborhood of the nominal point and do not, by themselves, describe how the admissible domain evolves as a parameter is varied over its full physically meaningful range. To address this, a complementary global sensitivity analysis was performed by sweeping each parameter individually, one at a time, while holding the remaining parameters fixed at their nominal values, and recording the corresponding response of the admissibility parameter ac. This procedure was repeated for the three area-ratio configurations already reported in the main text ($\lambda = 0.8, 1.0, 1.2$), for direct comparability with Figures 2 and 6.

Figure A2 confirms, over an extended stage range, the trend already visible in Figure 6: ac grows monotonically and supra-linearly with N for the three values of λ considered, crossing the admissibility boundary ac = 1 within the first one to two stages under the present operating conditions. This rapid growth follows directly from the quadratic dependence of the coefficient a on N through the angular-interaction term $N^2\alpha\lambda^2\sin^2\theta$, combined with the linear dependence of c on N, so that the product ac scales approximately as N^2 for sufficiently large N, exactly as anticipated by the asymptotic estimate of N_{crit} given in Equation (49). It is worth noting that, although the three curves remain close to one another for small N, the configuration with the largest area ratio (λ = 1.2) consistently produces the fastest growth of ac, and, therefore, the smallest admissible stage count, an effect that becomes more pronounced as N increases. This behavior is consistent with the positive elasticity of ac with respect to λ reported in Appendix A.1, and indicates that, under the inertia-dominated, low-Reynolds-number conditions of the present operating point, increasing the area ratio narrows rather than widens the admissible design space, in contrast with the asymptotic large − λ limit discussed in the main text, where the angular term eventually saturates.

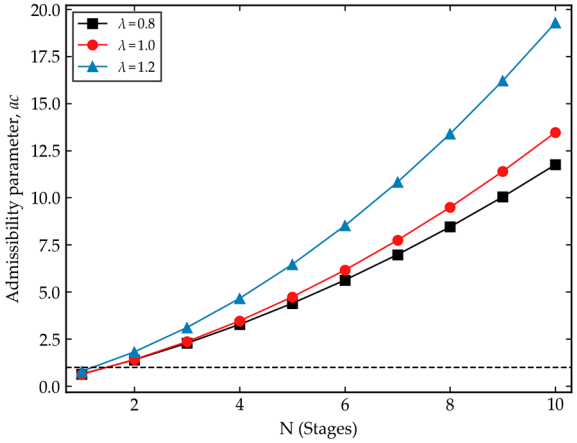


Figure A2. One-at-a-time sweep of the admissibility parameter ac as a function of the stage number N, for λ = 0.8, 1.0, and 1.2, at θ = 45°. The dashed horizontal line marks the admissibility boundary ac = 1. This sweep reproduces, in extended form, the same ac vs. N behavior reported in Figure 6 of the main text.

In contrast to the rapid growth observed for N, Figure A3 shows that ac varies only mildly with θ over the full physically relevant range of branch angles, remaining well below the admissibility boundary for all three values of λ considered. The curves exhibit a broad, gently varying profile, with ac decreasing slowly as θ increases beyond roughly 40 − 50°, which is consistent with the small magnitude of the local elasticity of ac with respect to θ reported in Appendix A.1. This behavior follows from the structure of the coefficient a, in which the angular-interaction term scales with $\sin^2\theta$, a bounded and slowly varying function over most of the domain, whereas the geometric term $1 + \lambda\cos\theta$ decreases monotonically with θ and partially offsets the growth of the angular contribution. Taken jointly with Figure A2, this result indicates that, within the present operating regime, the branch angle plays a comparatively secondary role in determining whether the formulation remains admissible, even though, as shown in Appendix A.1, it remains an important parameter for the magnitude of the diodicity itself once admissibility is satisfied.

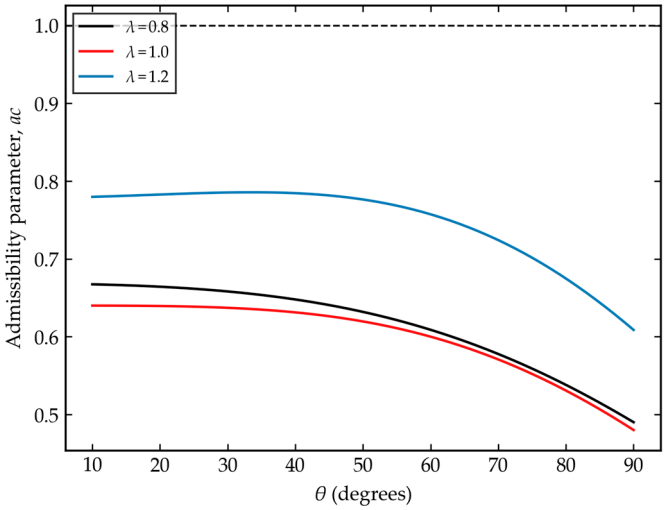


Figure A3. One-at-a-time sweep of the admissibility parameter ac as a function of the branch angle θ, for λ = 0.8, 1.0, and 1.2, at N = 1. The dashed horizontal line marks the admissibility boundary ac = 1.

Appendix A.3. Two-Parameter Admissibility Maps

While the one-at-a-time sweeps of Appendix A.2 isolate the marginal effect of each parameter, they do not reveal how the admissibility boundary itself migrates when two parameters are allowed to vary jointly. To complete the sensitivity assessment, two-dimensional admissibility maps were constructed by evaluating ac over a dense grid in the (λ, N) and (θ, N) planes, with the complementary parameter held at its nominal value in each case and superimposition of the contour ac = 1 that separates the admissible region (ac ≤ 1) from the inadmissible region (ac > 1).

The contrast between Figures A4 and A5 provides, in graphical form, the same conclusion already anticipated by the local elasticities and by the one-at-a-time sweeps. In the (λ, N) plane of Figure A4, the ac = 1 boundary is almost horizontal and confined to very low stage numbers across the entire range of λ explored, indicating that, for the present operating point, the admissible region is bounded primarily by N and is only weakly displaced by changes in λ; increasing λ does shift the boundary to slightly lower N, consistent with the positive elasticity of ac with respect to λ, but the effect is modest compared with the steep increase in ac with N itself. In the (θ, N) plane of Figure A5, the ac = 1 boundary is essentially flat across the full range of branch angles considered, confirming that θ has a negligible influence on the location of the admissibility boundary, in agreement with the near-zero elasticity reported in Appendix A.1 and with the mild variation in ac with θ observed in Figure A3. Taken together, Figures A1–A5 support a single, consistent conclusion: within the present reduced-order formulation, the admissible operating domain defined by ac ≤ 1 is governed almost entirely by the stage number N and the cumulative loss coefficient K_{base}, with the area ratio λ playing a secondary role and the branch angle θ playing only a marginal role in setting the boundary of admissibility, even though λ and θ remain the principal parameters controlling the magnitude of the diodicity once a configuration lies within the admissible domain. This separation between the parameters that govern admissibility and those that govern rectification strength is, in the authors' view, the most useful practical outcome of the present sensitivity analysis, since it indicates that, for design purposes, N and the cumulative hydraulic losses should be treated as the primary variables to constrain when verifying compliance with the admissibility condition of Equation (68), while λ and θ should be regarded as the primary variables to tune, within that admissible range, in order to maximize the rectification performance of the device.

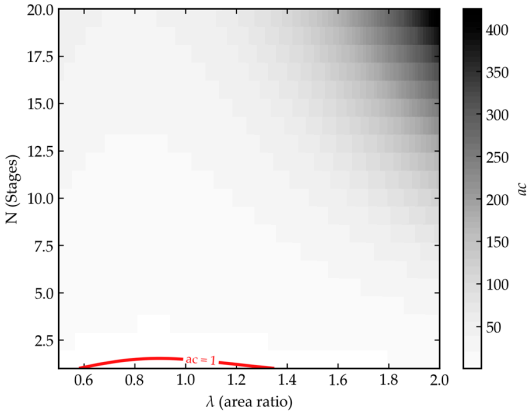


Figure A4. Admissibility map of ac as a joint function of the area ratio λ and the stage number N, at θ = 45°. The red contour marks the boundary ac = 1; the region below and to the left of the contour is admissible (ac ≤ 1), while the shaded region above and to the right is inadmissible (ac > 1).

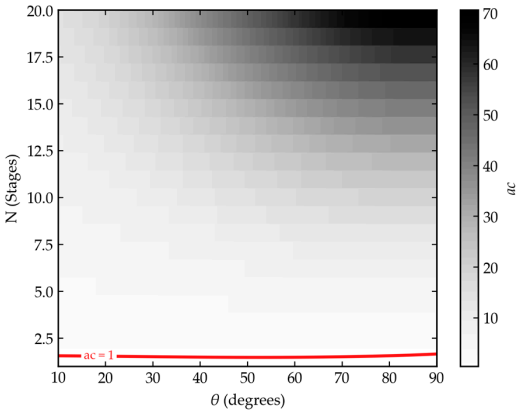


Figure A5. Admissibility map of ac as a joint function of the branch angle θ and the stage number N, at λ = 1.0. The red contour marks the boundary ac = 1.

It should be emphasized that the sensitivity ranking reported in this appendix is specific to the inertia-dominated, low-Reynolds-number operating point examined in the main text, for which K_{base} is comparatively large and the admissible stage range is correspondingly narrow. At higher Reynolds numbers, where the friction-dependent contribution K_{r0} decreases and K_{base} becomes smaller, the admissible domain widens and the relative influence of N, λ, and θ on ac is expected to redistribute accordingly, since the balance between the geometric term and the angular-interaction term in the coefficient a shifts as N_{crit} increases. The present appendix should, therefore, be read as a representative, fully reproducible illustration of the sensitivity methodology applicable to the proposed formulation, rather than as a universal ranking of parameter importance across the entire admissible operating space of the Tesla valve.

References

1. Tesla, N. Valvular Conduit. Patent 1,329,559, 3 February 1920.
2. Chen, L.; Su, C.; Li, S.; Ye, K. Design and diodicity enhancement mechanism of a double-baffle Tesla valve. *Int. J. Mech. Sci.* **2025**, *302*, 110575. [CrossRef]
3. Liu, Z.; Shao, W.Q.; Sun, Y.; Sun, B.H. Scaling law of the one-direction flow characteristics of symmetric Tesla valve. *Eng. Appl. Comput. Fluid Mech.* **2022**, *16*, 441–452. [CrossRef]
4. Jiang, E.; Wang, W.; Miao, J.; Zhang, H. Effect of the Tesla Valve on the heat transfer performance and the suppression of pressure drop oscillation in a liquid cooling loop. *Int. J. Therm. Sci.* **2025**, *207*, 109356. [CrossRef]
5. Jiang, H.; Tong, J.; Zhang, Y.; Zhao, Y. Flow characteristics inside rectangular Tesla valve with different width-to-narrow ratios. *Adv. Mech. Eng.* **2024**, *16*, 16878132241292404. [CrossRef]

6. Nguyen, Q.M.; Abouezzi, J.; Ristroph, L. Early turbulence and pulsatile flows enhance diodicity of Tesla's macrofluidic valve. *Nat. Commun.* **2021**, *12*, 2884. [CrossRef] [PubMed]
7. Liosis, C.; Papadatos, A.; Pagonis, D.N.; Peppa, S.; Sarris, I. Diodicity of MicroTesla Valves Under Various Re Numbers. *Micromachines* **2025**, *16*, 1329. [CrossRef] [PubMed]
8. Varnier, F.; Norouzikudiani, R.; Corsi, G.; Agostinelli, D.; Levin, I.; DeSimone, A. Hydraulic Asymmetries for Biological and Bioinspired Valves in Tubular Channels: A Numerical Analysis. *Biomimetics* **2026**, *11*, 87. [CrossRef] [PubMed]
9. Gamboa, A.R.; Morris, C.J.; Forster, F.K. Improvements in Fixed-Valve Micropump Performance Through Shape Optimization of Valves. *J. Fluids Eng.* **2005**, *127*, 339–346. [CrossRef]
10. Gamboa, A.R.; Morris, C.J.; Forster, F.K. Optimization of the Fixed-Geometry Valve for Increased Micropump Performance. *Fluids Eng.* **2003**, *259*, 525–534. [CrossRef]
11. Son, S.; Hwang, J.H. Application of Tesla Valve to Bidirectional Open-Channel Flows. *KSCE J. Civ. Eng.* **2024**, *28*, 1011–1025. [CrossRef]
12. Zeidan, M.; Németh, M.; Abhijith, G.R.; Wéber, R.; Ostfeld, A. Transient Flow Dynamics in Tesla Valve Configurations: Insights from Computational Fluid Dynamics Simulations. *Water* **2024**, *16*, 3492. [CrossRef]
13. Chou, C.Y.; Kuo, G.C.; Chueh, C.C. Numerical analysis of thermal-hydraulic influence of geometric flow baffles on multistage Tesla valves in printed circuit heat exchangers. *Appl. Therm. Eng.* **2024**, *251*, 123601. [CrossRef]
14. Hilborn, M.A.; Jauernig, K.A.; Pegg, M.J.; Haelssig, J.B. Analysis of Tesla valve geometric parameters for the optimization of diodicity within a flow control device. *Int. J. Heat Fluid Flow* **2026**, *120*, 110396. [CrossRef]
15. Liu, W.; Zhang, X.; Cao, Z.; Fang, K.; Yang, X. Comparative analysis of performance of different types of Tesla valves. *J. Phys. Conf. Ser.* **2024**, *2854*, 012103. [CrossRef]
16. Phi, H.B.; Bohm, S.; Runge, E.; Dittrich, L.; Strehle, S. 3D passive microfluidic valves in silicon and glass using grayscale lithography and reactive ion etching transfer. *Microfluid. Nanofluidics* **2023**, *27*, 55. [CrossRef]
17. Huang, X.; Anufriev, R.; Jalabert, L.; Watanabe, K.; Taniguchi, T.; Guo, Y.; Ni, Y.; Volz, S.; Nomura, M. A graphite thermal Tesla valve driven by hydrodynamic phonon transport. *Nature* **2024**, *634*, 1086–1090. [CrossRef] [PubMed]
18. Liu, Z.; Han, Q.; Han, J.; Zhang, Y.; Chen, X.; Li, W. Flow boiling in a relatively large copper heat sink comprised of Tesla microchannels. *Int. J. Heat Mass Transf.* **2025**, *236*, 126366. [CrossRef]
19. Yadav, A.K.; Ram Gopal, M.; Bhattacharyya, S. Transient analysis of subcritical/supercritical carbon dioxide based natural circulation loops with end heat exchangers: Numerical studies. *Int. J. Heat Mass Transf.* **2014**, *79*, 24–33. [CrossRef]
20. Du, G.; Basem, A.; Othman, N.A.; Sinnah, Z.A.B.; Alhumaid, S.; Ayadi, M.; Albalawi, H.; Ali, H.E.; Alkhalaf, S.; AL Garalleh, H. Optimizing thermo/hydro-Diodic performance (T/H-DP) of Tesla valve designs by artificial neural network (ANN) and genetic algorithm (GA); a numerical simulation. *Int. Commun. Heat Mass Transf.* **2025**, *169*, 109711. [CrossRef]
21. Hai, T.; Rahman, M.A.; Aksoy, M.; Zhou, J.; Alenazi, M.J.F.; Singh, N.S.S.; Zain, J.M.; Jawawi, D.N.A. Investigating the performance of the Tesla valve channel in a photovoltaic thermal system through numerical simulation: Evaluation from the standpoint of thermodynamic laws. *Int. Commun. Heat Mass Transf.* **2024**, *159*, 108197. [CrossRef]
22. Wischhoff, O.P.; Holm, J.R.; Shankar, S.S.R.; Bienhold, G.J.; Jiang, J.J. Efficacy of a Tesla Valve Straw in a Semi-Occluded Vocal Tract Exercise in a Normal-Voiced Population. *J. Voice* **2025**. [CrossRef] [PubMed]
23. Wiley, S.; Huang, H.P. The Effect of Bifurcated Geometry on the Diodicity of Tesla Valves. *Fluids* **2024**, *9*, 294. [CrossRef]
24. Shakaib, M.; Ehtisharn ul Haq, M.; Fakhir Hasani, S.M. Effect of Tesla valve geometry on unsteady flow behavior and pressure drop. *Mem. Investig. Ing.* **2025**, *29*, 54–73. [CrossRef]
25. Guo, H.; Tian, S.; Wang, L.; Xiao, C.; Pan, Y.; Xie, W.; Yang, S. Influence of Structural Parameters of Tesla Valve Flow Field on Performance of Fuel Cells. *Energies* **2024**, *17*, 4442. [CrossRef]
26. Shinde, N.; Salema, Z.; Sakarwala, B. An Investigation of Non-Return Valves as Possible Sources of Pump Failure and A Comparative Analysis with Tesla Valves. *Int. J. Eng. Res. Technol.* **2020**, *9*, 71–80.
27. Truong, T.-Q.; Nguyen, N.-T. Simulation and Optimization of Tesla Valves. *Nanotech* **2003**, *1*, 147–173.
28. Purwidyantri, A.; Prabowo, B.A. Tesla Valve Microfluidics: The Rise of Forgotten Technology. *Chemosensors* **2023**, *11*, 256. [CrossRef]
29. Zhu, S.; Wang, P.; Liu, L.; Ding, C. Influence of Baffle Location on the Diodicity of Tesla Valves. *Appl. Sci.* **2025**, *15*, 5526. [CrossRef]
30. Sparrow, A.; Isley, J.; Smith, W.; Gannon, A. Geometric Optimization of a Tesla Valve Through Machine Learning to Develop Fluid Pressure Drop Devices. *Fluids* **2025**, *10*, 255. [CrossRef]
31. Zhang, Y.-L.; Tong, J.-B.; Zhu, Z.-C. Numerical calculation of forward and reverse flow in Tesla valves with different longitudinal width-to-narrow ratios. *Sci. Rep.* **2023**, *13*, 12496. [CrossRef] [PubMed]
32. Nobakht, A.Y.; Shahsavan, M.; Paykani, A. Numerical Study of Diodicity Mechanism in Different Tesla-Type Microvalves. *J. Appl. Res. Technol.* **2013**, *11*, 876–885. [CrossRef]

Disclaimer/Publisher's Note: The statements, opinions and data contained in all publications are solely those of the individual author(s) and contributor(s) and not of MDPI and/or the editor(s). MDPI and/or the editor(s) disclaim responsibility for any injury to people or property resulting from any ideas, methods, instructions or products referred to in the content.